electronics

MDPI

Article

EEG-Based Brain Dynamics in Motor Execution and Imagery: Spectral Analysis with Potential Applications in Neurorehabilitation

Audrey Rah * and Yuhua Chen

Department of Electrical and Computer Engineering, University of Houston, Houston, TX 77204, USA; yuhuachen@uh.edu

* Correspondence: arahimi@uh.edu

Abstract

This offline study examines alpha and beta spectral differences around the task annotations of the PhysioNet Electroencephalography (EEG) Motor Movement/Imagery Dataset. Motor-cortex EEG was analyzed from the PhysioNet motor-execution and motor-imagery recordings. The time origin was the dataset task annotation (T1 or T2), which marks the instructed target interval rather than independently measured movement onset. The primary one-second window, from -1.0 to 0.0 s, precedes the task annotation and lies in the preceding rest block when that block fully contains it. Spectral power features in the alpha and beta frequency bands were computed using Welch's method. Subject-wise z-score normalization was applied prior to statistical analysis. A comprehensive statistical evaluation was performed, including non-parametric group comparisons, pairwise post hoc tests with Bonferroni correction, effect size estimation, bootstrap confidence intervals, normality assessment, and rank correlation analysis. The original 109-subject Kruskal–Wallis contrast is significant ($H_\alpha = 74.79$, $p \ll 0.001$; $H_\beta = 289.01$, $p \ll 0.001$). Reanalysis established that these alpha and beta power differences compare the end of rest with the end of the preceding task, rather than a measured pre-movement interval with rest. Under the Methods-faithful per-trial ERD/ERS definition, alpha ERD did not differ significantly across rest/left/right ($H = 3.95$, $p = 0.139$) and is therefore not treated as a primary confirmed finding. Supplementary subject-held-out classification (107 participants) yielded an AUC of 0.595 for post-cue versus pre-cue rest discrimination, while pre-cue prediction of the upcoming hand remained at chance after sequence control. These findings do not establish limb-specific intention detection before movement. These findings characterize sensorimotor EEG dynamics and provide a foundation for future research on EEG-informed neurorehabilitation.

Keywords: electroencephalography; brain–computer interface; motor execution; motor imagery; cue-locked spectral power; event-related desynchronization; EEG spectral analysis

Check for updates

Academic Editor: Jichai Jeong

Received: 16 September 2026
Revised: 26 October 2026
Accepted: 28 October 2026
Published: 4 Novermber 2026

Copyright: © 2026 by the authors. Licensee MDPI, Basel, Switzerland. This article is an open access article distributed under the terms and conditions of the Creative Commons Attribution (CC BY) license.

1. Introduction

Neurological disorders associated with impaired motor control remain one of the leading causes of long-term disability worldwide, frequently resulting in reduced voluntary movement and loss of independence in daily activities [1,2]. Effective neurorehabilitation relies on repetitive, task-specific training combined with timely and meaningful feedback to facilitate neuroplasticity and motor re-learning [3,4]. In this context, virtual reality

(VR)-based rehabilitation has emerged as a promising approach, providing immersive, structured, and engaging environments that enable controlled task execution and real-time feedback delivery [5–7].

Figure 1 summarizes the offline Electroencephalography (EEG) analysis workflow and its potential future applications in VR-based neurorehabilitation.

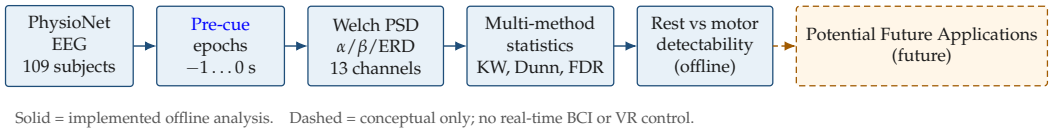


Figure 1. Graphical abstract summarizing the offline workflow from PhysioNet EEG acquisition through annotation-locked temporal segmentation, spectral feature extraction, and multi-method statistical comparison. The pre-cue analysis window extends from −1 to 0 s relative to the dataset task annotation. Navy boxes and solid arrows represent implemented offline analysis steps, while the amber dashed box and arrow indicate conceptual future applications in VR-based neurorehabilitation that were not implemented. The dashed elements do not represent real-time BCI or VR control.

Recent systematic reviews report generally positive outcomes of VR-based interventions on motor recovery and functional performance, although variability in implementation and system design remains [2,8]. Feedback is an important component of motor learning and neurorehabilitation, reinforcing performance through knowledge of results and knowledge of performance [3,9,10]. However, a fundamental limitation arises in early-stage recovery, where voluntary motor output may be extremely weak or absent despite the presence of underlying motor intention [3]. In such cases, VR systems that rely on observable movement fail to detect user intent, resulting in a lack of reinforcement and reduced engagement.

This limitation motivates further investigation of EEG signals associated with motor execution and imagery, particularly their temporal and spectral characteristics.

Although considerable progress has been made in VR-based rehabilitation and EEG-based brain–computer interfaces (BCIs), further investigation is needed to better understand the temporal and spectral characteristics of motor-related EEG activity. Examining these neural patterns may help identify relevant EEG features and provide a basis for future research on EEG-informed feedback in VR-based neurorehabilitation.

Recent work has explored the concept of detecting weak signals associated with early intent, particularly in VR-based behavioral sensing systems [11]. Sensor-assisted VR architectures have demonstrated that combining behavioral indicators with minimal physiological sensing can improve detection sensitivity while maintaining low system complexity [12]. In addition, adaptive detection frameworks have highlighted the importance of modeling low-amplitude signal variations and optimizing threshold selection under noisy conditions [13].

These studies illustrate the challenges of analyzing low-amplitude signals and the importance of appropriate signal-processing methods.

BCI technologies provide a direct pathway to capture neural activity associated with motor intention. A BCI is a direct communication pathway between the brain and an external device, in which measured neural activity is translated into control commands for assistive, rehabilitative, or communication systems without dependence on normal neuromuscular output [14,15]. The concept of direct brain-controlled communication was introduced by Vidal (1973), who demonstrated the feasibility of real-time EEG-based device control, establishing the foundation for subsequent BCI research [16]. In the present study, EEG signals are analyzed offline as annotation-locked EEG spectral analysis; no external device is controlled and no real-time decoding is performed.

EEG, as a non-invasive modality, enables the measurement of brain signals related to motor planning, motor imagery, and execution [15]. Publicly available datasets, such as the PhysioNet EEG Motor Movement/Imagery database, provide labeled EEG recordings of motor tasks and imagined movements, enabling the systematic investigation of neural patterns associated with intention [17]. Motor imagery signals are particularly relevant in rehabilitation contexts, as they represent internally generated motor commands without physical movement, closely reflecting early-stage recovery scenarios. Despite advances in EEG-based BCI systems, most existing studies focus on the classification of well-defined motor imagery tasks or detection of neural activity after movement onset. Relatively limited attention has been given to the detection of very weak pre-movement neural signals that occur prior to movement initiation.

These signals are typically low in amplitude, embedded in noise, and difficult to detect using conventional processing approaches. Further characterization of motor-related EEG activity may support future research on EEG-informed feedback, including potential applications in VR-based neurorehabilitation.

This concept extends the idea of micro-intent detection from biomechanical sensing to the neural domain. That motivation is prospective. The analyses below do not establish that such intention-triggered feedback was implemented or validated. Unlike most previous studies that primarily emphasize classification accuracy or online control, the present work focuses on annotation-locked EEG spectral analysis of labeled rest and motor intervals. This perspective offers a methodological foundation for future research integrating sensorimotor EEG analysis with VR-based neurorehabilitation approaches. In this study, we investigate late-rest versus late-task EEG spectral differences, providing insights into sensorimotor dynamics that may support future developments in VR-based neurorehabilitation. A computational approach is adopted using open EEG datasets to extract pre-cue windows preceding the dataset task annotation. Signal processing techniques are applied to analyze low-amplitude neural activity and evaluate its detectability under realistic conditions. The implemented study consists of offline EEG spectral estimation, statistical comparison, preceding-block analysis, and supplementary cue-locked classification. It does not include a real-time intention decoder, an implemented VR system, or clinical validation. "Detection" in the original analysis meant a significant group contrast, not single-trial classification. The findings characterize cue-locked sensorimotor EEG activity and may inform future investigations of EEG-based feedback, including potential applications in VR-based neurorehabilitation. Further studies are needed to validate these features in interactive rehabilitation settings.

The contributions of this work are as follows:

1. A cue-locked description of alpha and beta power in the PhysioNet execution and imagery runs.
2. A preceding-block reanalysis showing that the original −1 to 0 s motor label is late rest.
3. Supplementary evidence that power falls after the cue and that a contralateral slow potential appears after the cue.
4. A methodological foundation for exploring EEG-informed feedback strategies in potential future neurorehabilitation research.

The novelty of this work is primarily methodological and application-oriented rather than data- or algorithm-centric. The present study focuses on offline EEG analysis and provides a basis for future research exploring potential applications in VR-based neurorehabilitation. Furthermore, it extends group-level statistical comparisons through an exploratory feature-ranking and biomarker-selection analysis, complementary statistical evaluation of EEG spectral differences, and consideration of potential future VR-based neurorehabilitation applications. The analysis focuses on the pre-cue window (−1.0 to 0.0 s

relative to the task annotation) and examines spectral differences across annotated rest and motor conditions, rather than prioritizing left-versus-right classification. Preceding-block analysis further establishes that the original condition differences reflect late-rest versus late-task activity and cannot be interpreted as verified pre-movement intention signals. Previous BCI studies have examined neural decoding and online control [14,18], while VR rehabilitation research has addressed therapeutic outcomes and patient engagement [19]. The present study examines the statistical characteristics of low-amplitude sensorimotor EEG signals using complementary analytical methods, including non-parametric comparisons, effect-size estimation, and supplementary cue-locked analyses. Although previous research has investigated motor-related neural activity and EEG-based classification, reliable interpretation of EEG features remains important before their use in decoding and control applications [14,20,21]. Accordingly, this work contributes a statistical characterization of annotation-locked EEG spectral differences, an exploratory assessment of feature relevance, and an evaluation of temporal alignment. These findings may provide a basis for future investigations of EEG-informed feedback, including potential applications in VR-based neurorehabilitation.

The remainder of this paper is organized as follows: Section 2 reviews recent studies on VR rehabilitation, EEG-based brain–computer interfaces, motor imagery, and weak neural signal detection, highlighting the research gap addressed in this work. Section 3 presents the PhysioNet dataset, EEG preprocessing pipeline, spectral feature extraction, statistical analysis framework, and computational methodology used to evaluate annotation-locked labeled-condition spectral differences. Section 4 reports the experimental findings using complementary statistical analyses, including non-parametric hypothesis testing, bootstrap confidence intervals, permutation testing, linear mixed-effects modeling, and false discovery rate correction. Section 5 discusses the potential relevance of these findings to potential future neurorehabilitation research, outlines the study limitations, and identifies directions for future research. Finally, Section 6 summarizes the main conclusions and contributions of the proposed framework.

2. Related Work

VR has increasingly been adopted as an adjunct to conventional rehabilitation due to its ability to deliver repetitive, task-oriented training within controlled and interactive environments [7]. By enabling structured task execution and real-time feedback, VR systems can support intensive rehabilitation while maintaining patient engagement. Recent systematic reviews and meta-analysis report that VR-based interventions can improve balance, walking ability, and functional performance in rehabilitation populations, although reported outcomes vary depending on protocol design and immersion level [2,8]. Broader evidence syntheses further emphasize the heterogeneity of VR implementations, including differences in hardware configurations, feedback strategies, and training dosage [22,23]. Patient-centered evaluations also indicate that VR-based rehabilitation is generally well tolerated and acceptable across different recovery stages [24]. Despite these encouraging findings, clinical outcomes remain inconsistent across studies. One important reason is that many current VR systems still depend on measurable physical movement before feedback can be delivered. This limitation becomes particularly important for individuals with severe motor impairment, where voluntary movement may be minimal or absent during the early stages of rehabilitation. A central mechanism underlying VR rehabilitation efficacy is augmented feedback, which reinforces motor learning through immediate performance cues and knowledge of results [9,10]. Closed-loop and adaptive training approaches have been proposed to dynamically adjust task difficulty based on user performance, enabling personalized rehabilitation particularly for individuals with severe impairments [25]. Such

adaptive strategies align with motor learning principles, where timely reinforcement and graded challenge are essential for promoting neuroplasticity and functional recovery [4].

Recent studies in EEG-based BCI systems have demonstrated the feasibility of detecting neural activity associated with motor intention, particularly within motor imagery and motor preparation paradigms [15]. Event-related desynchronization (ERD) and event-related synchronization (ERS) have been widely reported as key neural signatures of motor planning and preparation, including ERD in the alpha band and modulation of beta-band activity [26,27]. These spectral changes reflect cortical activation patterns that emerge prior to overt movement execution, making them relevant for early intention detection.

The historical development of anticipatory motor-related EEG phenomena spans early readiness potential observations [28], contingent negative variation [29], and subsequent spectral-domain formulations of ERD [26]. Early investigations of anticipatory EEG patterns and their relevance to brain-controlled systems were reported by Bozinovska et al. (1992), preceding modern motor imagery BCI frameworks [15,30].

Pfurtscheller and Neuper [31] investigate motor imagery and ERD, and Schalk et al. [32] describe the BCI2000 software platform. Those references do not supply independently measured movement-onset timing for the present PhysioNet files and are not used here as evidence that this study detected pre-movement intention. However, most existing work focuses on the classification of motor imagery tasks or detection of neural activity after movement onset, while the detectability of very weak pre-movement signals remains unexplored.

From a rehabilitation perspective, the reliability and temporal interpretation of EEG features remain important considerations. Future applications of EEG-informed feedback will require validation of these features in relation to measured motor events. From a signal-processing perspective, the detection of weak EEG signals presents significant challenges due to low signal amplitude, high variability, and the presence of background noise [15]. Robust statistical methods, including non-parametric analysis techniques, have been emphasized as essential tools for reliably characterizing low-amplitude neural activity without relying on strict distributional assumptions [33]. These approaches enable consistent identification of subtle neural patterns under realistic and noisy conditions.

Beyond neural signal processing, VR has also been conceptualized as a measurement platform capable of capturing behavioral and physiological signatures with minimal hardware overhead [11]. Sensor-assisted VR architectures demonstrate that combining behavioral indicators with lightweight physiological sensing can improve detection sensitivity while maintaining system simplicity [12]. Related work on physiological sensing in VR has also shown that temperature-adjusted electrodermal activity can improve the robustness of stress-related signal interpretation under varying physiological conditions [34]. Adaptive detection frameworks further emphasize the importance of threshold calibration and signal normalization when dealing with low-amplitude signals under noisy conditions [13].

Despite these advances, the interpretation of low-amplitude EEG activity remains challenging, particularly when neural responses are aligned to task annotations rather than measured movement onset.

Motor learning theory highlights the importance of repetition, task specificity, and progressive challenge in promoting cortical reorganization [4,35]. The identification of reliable motor-related neural features may support future research on feedback strategies for individuals with limited voluntary movement [4]. Many existing studies emphasize classification accuracy rather than the detectability of the underlying neural signal. Understanding whether these weak signals can be detected reliably is an important step before developing more advanced decoding algorithms or real-time BCI control systems.

Taken together, the existing literature supports the feasibility of detecting motor-related neural activity prior to movement execution while highlighting the methodological challenges associated with weak signal detection [15,33]. However, a systematic evaluation of the detectability of very low-amplitude pre-movement EEG signals remains limited [31].

Addressing this gap is essential for enabling the development of BCI-driven rehabilitation systems capable of delivering feedback based on neural intention rather than completed motor execution [15].

Prior studies using the PhysioNet EEG Motor Movement/Imagery database predominantly target multi-class motor imagery classification (e.g., left versus right versus feet) using spatial filtering such as common spatial pattern (CSP), deep learning, or end-to-end decoding across full trial durations [15]. Consequently, the difference between the present study and prior PhysioNet-based investigations lies not in the dataset itself but in the research question being addressed. Comparison with recent studies reveals that the primary distinction of the proposed framework lies in its detectability-oriented perspective: while most prior work evaluates how accurately motor states can be classified, the present study investigates labeled-condition spectral differences in an annotation-locked pre-cue window. The present work differs in three respects: (1) analytical focus on the pre-cue window (-1.0 to 0.0 s relative to the task annotation) rather than entire-trial classification, (2) primary detection objective of motor-related activation versus rest, aligned with early-stage rehabilitation where discriminating labeled motor intervals from rest is prioritized over fine motor class discrimination and (3) emphasis on statistical detectability under weak signal-to-noise conditions using convergent non-parametric validation rather than reporting classification accuracy alone.

Table 1 provides a design-oriented comparison with movement-intention EEG studies. It distinguishes the movement-alignment event, availability of movement-onset measurements, evaluation paradigm, and reported metric type. Performance values are not compared, because the tasks, alignment events, and metrics differ. Their single-trial detection results are not interchangeable with the cue-locked group-level spectral comparisons or with the supplementary classification AUCs reported here. Group-level Kruskal–Wallis statistics are therefore not treated as comparable to single-trial detection accuracies.

Table 1. Design comparison with studies of movement intention. Performance values are not compared, because the tasks, alignment events, and metrics differ.

Study	Role	Alignment/Movement Measure	Design Notes
Blankertz et al. [20]	CSP tutorial/methods paper	Not a PhysioNet movement-intention analysis	Identified as a methodological reference rather than a pre-movement detection benchmark.
Schalk et al. [32]	BCI2000 software description	Not a detection result	Identified as a software reference rather than a pre-movement detection benchmark.
Niazi et al. [36]	Single-trial MRCP detection	EMG or equivalent movement timing	Self-paced; detection before or near movement, which cue-locked files cannot test.
Bai et al. [37]	Online prediction of voluntary movement	EMG-confirmed self-paced wrist extension	Movement confirmed independently of the EEG cue.
Lew et al. [38]	Readiness-potential detection	Self-paced reaching; about 500 ms before onset	Intention locked to measured movement onset.
Jochumsen et al. [39,40]	Single-trial MRCP/ idle-versus-movement EEG	Measured or self-paced movement event	Clinical cohorts; single-trial detection relative to a movement event.
Dong et al. [41]	Pre-movement intention decoding	Measured or self-paced movement event	Not interchangeable with cue-locked group contrasts.

Table 1. *Cont.*

Study	Role	Alignment/Movement Measure	Design Notes
Crell et al. [42]	Online MRCP-based BCI	Measured movement event	Online communication task; not an accuracy benchmark for the present study.
Zhang et al. [43]	MRCP decoding at different speeds	Measured movement event	Single-trial decoding relative to movement.
Present study	Offline cue-locked spectral comparison	Task annotation T1/T2; no EMG	Group contrast and supplementary single-trial AUCs are not accuracy figures on the same scale as the studies above.

3. Methodology

This study evaluates labeled-condition spectral differences in annotation-locked pre-cue EEG windows, with potential relevance to future neurorehabilitation research. This study does not perform clinical experiments; instead, it evaluates detectability using computational analysis based on real EEG recordings. The implemented analysis tests labeled-condition spectral differences locked to the dataset task annotation. It does not measure movement onset and does not demonstrate pre-movement intention detection.

EEG signals were not translated into real-time commands for any external actuator, display, or rehabilitation interface in the present study. The proposed framework integrates four components: (1) physiological EEG recordings, (2) pre-cue window extraction, (3) spectral feature modeling, and (4) statistical detectability analysis.

3.1. Analysis Framework and System Architecture

The primary analysis interval (−1.0 to 0.0 s) provides one second for Welch PSD estimation immediately before the dataset task annotation. Previous studies have reported ERD, mu-rhythm suppression, and beta-band modulation during motor preparation [26,27]. Those reports used independently timed movement events and are not treated here as verification of PhysioNet T1/T2 alignment.

A conceptual future stage illustrates how independently validated EEG features could be explored for adaptive feedback in VR-based neurorehabilitation.

The system architecture presents the offline EEG analysis workflow alongside a prospective extension toward VR-based neurorehabilitation. Solid boxes represent the analytical workflow, while dashed boxes indicate opportunities for future integration.

Figure 2 presents the overall architecture used in this study. The workflow begins with validation of the PhysioNet EEGMMIDB recordings and proceeds through the selected sensorimotor channels, temporal segmentation, spectral feature extraction, subject-wise normalization, and statistical validation. The final implemented stages interpret the resulting pre-cue EEG features and generate the corresponding figures and tables. The dashed BCI–VR component is shown separately to indicate that real-time feedback and VR actuation are not part of the present implementation.

Figure 3 provides a more detailed view of the EEG processing sequence implemented in the analysis. The validated recordings are processed using the thirteen-channel sensorimotor montage and segmented into baseline and pre-cue intervals. Welch PSD is then used to extract the spectral features, followed by subject-wise normalization and statistical analysis. This figure therefore summarizes how the raw EEG recordings are transformed into the feature values used for the subsequent detectability analysis.

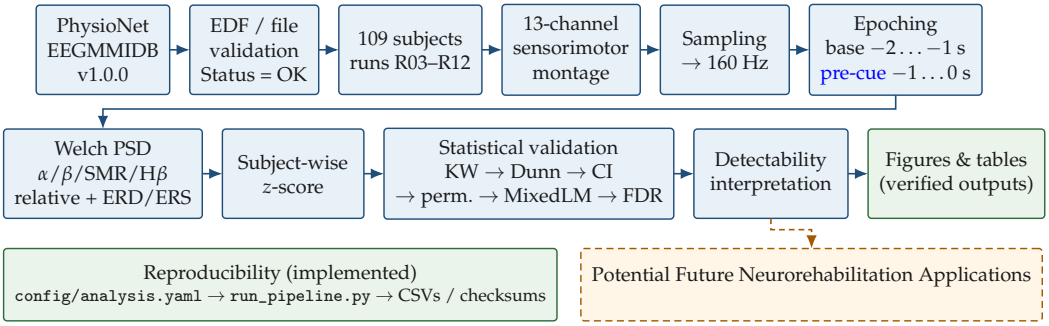


Figure 2. Overall system architecture of the Methods-faithful annotation-locked detectability framework. The implemented flow proceeds from PhysioNet EEGMMIDB file validation through 109 subjects, the 13-channel sensorimotor montage, 160 Hz sampling handling, baseline ($-2 \ldots -1$ s) and pre-cue ($-1 \ldots 0$ s) epoching, Welch spectral features, subject-wise normalization, multi-method statistical validation, detectability interpretation, and manuscript figure/table generation. Conceptual BCI–VR feedback is shown as a future stage only; no real-time control or VR actuation is implemented. Blue boxes and solid arrows indicate the implemented workflow, green boxes indicate verified outputs and reproducibility, and the orange dashed elements represent future applications. Ellipses indicate time intervals, not missing information.

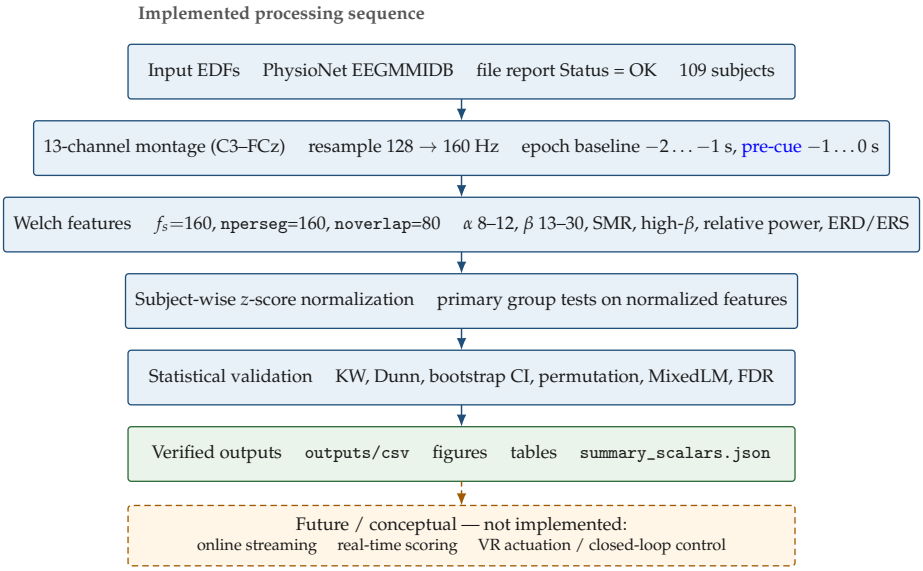


Figure 3. EEG processing pipeline corresponding to the implemented code path (`pipeline_core.extract_features`, Welch band-power/ERD extraction, subject-wise z-score normalization, and statistical interpretation). Future online streaming, real-time scoring, and VR actuation blocks are marked as not implemented. Blue boxes and solid arrows indicate the implemented processing sequence, the green box indicates verified outputs, and the orange dashed box and arrow represent conceptual future functions. The ellipses indicate time intervals rather than missing scientific information.

Virtual reality is not an experimental condition in this study. The statistical procedures used in the Results remain described in Section 3 and are not repeated as diagrams. Benjamini–Hochberg correction controls the false discovery rate, whereas the Bonferroni correction used for Dunn's post hoc comparisons controls the family-wise error rate within the relevant comparison family.

3.2. Physiological EEG Data

EEG signals were obtained from the PhysioNet EEG Motor Movement/Imagery dataset [17]. The dataset contains EEG recordings from 109 subjects performing motor exe-

cution and motor imagery tasks. The recordings include labeled conditions corresponding to rest, left-hand movement, and right-hand movement.

All 109 subjects included in PhysioNet EEG Motor Movement/Imagery Database version 1.0.0 were retained. No subject exclusion was applied beyond the dataset's own availability criteria, and no demographic-, performance-, or signal-quality-based filtering was performed. Each subject contributed multiple runs corresponding to rest, left-hand motor execution/imagery, and right-hand motor execution/imagery conditions as defined by the dataset protocol. Recordings were predominantly sampled at 160 Hz using the international 10–10 electrode montage; eighteen validated files recorded at 128 Hz were resampled to 160 Hz so that the Welch settings ($f_s = 160$ Hz, `nperseg` = 160, `noverlap` = 80) apply uniformly. A native-rate sensitivity analysis confirmed unchanged Kruskal–Wallis significance conclusions for alpha power, beta power, and alpha ERD. Analysis was restricted to thirteen sensorimotor electrodes (C3, C1, Cz, C2, C4, CP1, CP3, CPz, CP2, CP4, FC1, FC2, and FCz) covering primary motor and premotor cortical regions. These channels were selected because they overlie cortical areas most consistently associated with motor preparation, motor execution, motor imagery, ERD, and beta-band modulation. Channel selection followed established motor-BCI conventions, prioritizing electrodes overlying primary motor cortex (M1), supplementary motor area (SMA), and premotor cortical regions. These areas are known to exhibit prominent ERD and beta-band modulation during motor preparation, motor execution, and motor imagery. Restricting the analysis to sensorimotor electrodes reduces dimensionality while focusing on cortical regions with the highest expected relevance to intention-related neural activity [26,27,44].

To further evaluate the consistency of the prespecified sensorimotor montage with the observed data, we performed a supplementary post hoc comparison across all 64 EEG electrodes. As summarized in Table 2, the prespecified thirteen-channel sensorimotor montage exhibited a higher mean absolute Rest-versus-Motor effect size than the remaining electrodes (0.1253 versus 0.0666, respectively), with 11 of the 13 selected channels ranking among the 20 highest-ranked electrodes. This supplementary analysis was conducted only to assess the consistency of the prespecified channel selection with the observed data and was not used to determine channel selection or modify the primary analysis pipeline.

Figures 4 and 5 provide supporting visualizations of the same in Table 2 channel-relevance values. They do not redefine the primary thirteen-channel montage, do not introduce new statistics, and are not used to alter channel selection.

C3 and C4, the canonical contralateral primary motor cortex electrodes, were explicitly included. Although group-level features were computed as a montage mean, both electrodes contributed directly to all reported spectral and ERD/ERS measures. Separate C3-versus-C4 lateralized comparisons were not the primary inference target of this study.

These recordings were collected under controlled experimental protocols and provide physiologically realistic neural activity associated with motor planning and execution. Such signals therefore serve as a suitable basis for analyzing weak neural activation events.

Demographic attributes such as age and gender were not used in the present analysis because the focus of this study is on signal detectability rather than subject-specific clinical characteristics.

For the present analysis, EEG segments corresponding to the annotation-locked pre-cue window were selected. These segments represent labeled rest and motor intervals; they are not independently timed movement-onset recordings. Using real physiological recordings ensures that the evaluation reflects realistic neural variability present in neurorehabilitation environments.

Table 2. Supplementary post hoc relevance analysis of the thirteen prespecified sensorimotor electrodes. Effect sizes represent Rest-versus-Motor Cohen's d values for subject-normalized α and β power. Mean absolute effect was calculated as the mean of the absolute α and β effect sizes. The analysis was performed only as a supplementary consistency check and was not used for channel selection.

Channel	d_α	d_β	Mean $\lvert d \rvert$	Overall Rank
C3	0.107	0.236	0.172	1
CP3	0.105	0.218	0.162	2
C4	0.101	0.214	0.157	3
FCz	0.056	0.215	0.136	5
C1	0.061	0.194	0.128	6
FC2	0.055	0.199	0.127	7
FC1	0.053	0.199	0.126	8
CP4	0.087	0.165	0.126	9
C2	0.057	0.178	0.117	14
CP1	0.068	0.156	0.112	18
Cz	0.047	0.175	0.111	20
CP2	0.045	0.113	0.079	29
CPz	0.038	0.106	0.072	31
Mean absolute effect, selected 13			**0.1253**	–
Mean absolute effect, remaining 51			**0.0666**	–

Note: Boldface identifies the two summary rows. An en dash (–) indicates that an overall rank is not applicable to these rows.

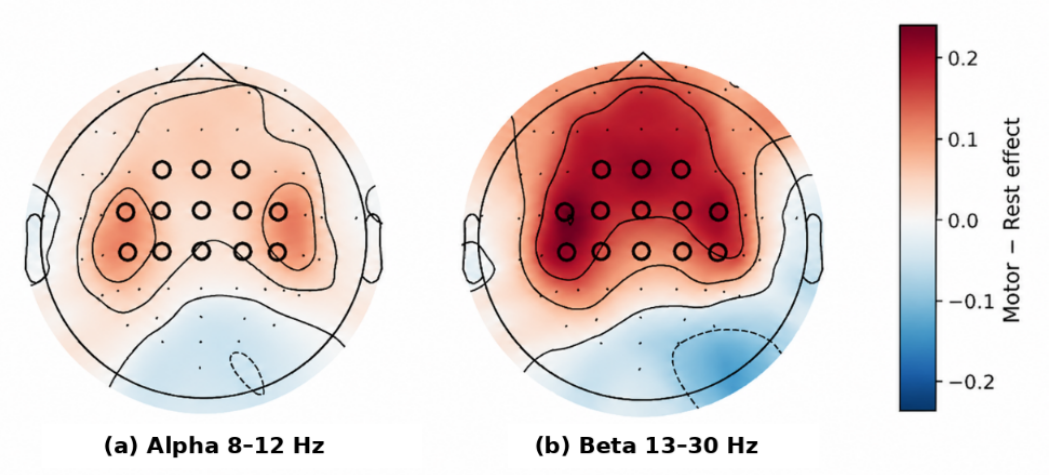


Figure 4. Supporting scalp topography of Motor−Rest channel effects for alpha (8–12 Hz) and beta (13–30 Hz), mapped from the existing Table 2/64-channel relevance outputs. Black circles mark the predefined thirteen-channel sensorimotor montage used in the primary analysis. Solid and dashed black lines represent interpolated iso-effect contours and do not indicate statistical significance. This figure is a spatial visualization of existing supplementary effect sizes and is not a new primary analysis.

3.3. EEG Preprocessing Pipeline

The preprocessing pipeline comprised the following steps, applied uniformly across all subjects and conditions:

1. Extraction of task-labeled epochs from PhysioNet European Data Format (EDF) recordings using the dataset-provided event annotations.
2. Temporal segmentation into a baseline window (−2.0 to −1.0 s) and a primary analysis window (−1.0 to 0.0 s), both defined relative to the dataset task annotation ($t = 0$ at the start of T1 or T2). These windows are not claimed to isolate movement onset or the onset of motor intention.
3. Constant detrending (DC offset removal)

4. Welch PSD estimation with band power integrated within alpha (8–12 Hz) and beta (13–30 Hz) limits.
5. Subject-wise z-score normalization was applied to reduce inter-subject variability prior to statistical analysis.

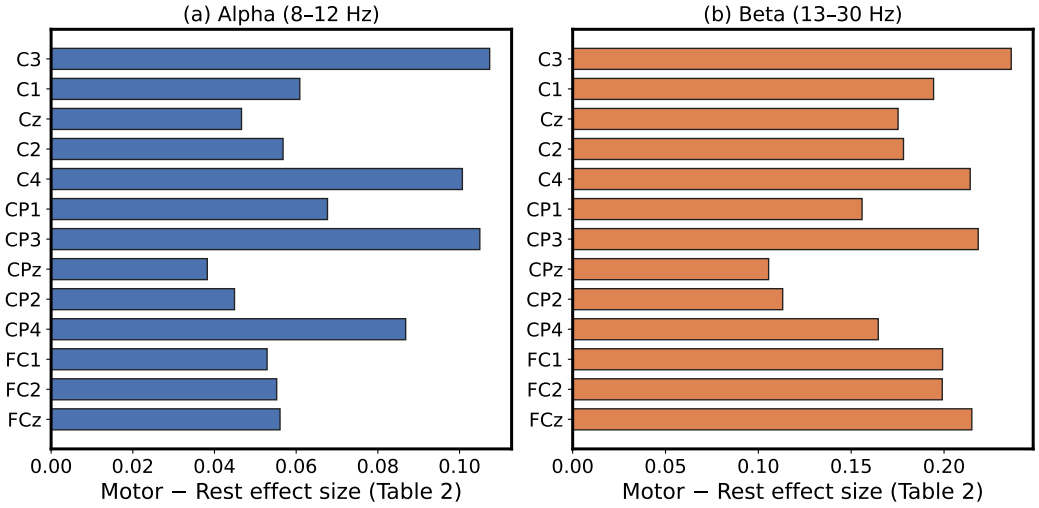


Figure 5. Supporting visualization of Motor−Rest effect sizes on the predefined thirteen sensorimotor channels (C3, C1, Cz, C2, C4, CP1, CP3, CPz, CP2, CP4, FC1, FC2, and FCz). Values are identical to Table 2 (Selected13). The primary montage is unchanged.

Band power was computed independently for each sensorimotor electrode within each temporal window; features were aggregated as the montage mean prior to subject-wise normalization. For each selected channel, Welch PSD was computed independently within the baseline and pre-cue windows. Alpha (8–12 Hz) and beta (13–30 Hz) band-power values were extracted at the channel level and subsequently averaged across the thirteen-electrode sensorimotor montage to generate a single feature representation per trial prior to subject-wise normalization. No supplementary independent component analysis (ICA), artifact subspace reconstruction (ASR), manual trial rejection, common average reference (CAR), Laplacian filtering, or CSP preprocessing was applied. The recordings were obtained under controlled laboratory conditions using the standardized PhysioNet acquisition protocol. Subject-wise normalization addresses inter-subject scaling differences and is distinct from artifact rejection. The objective was to evaluate labeled-condition spectral differences using a standardized and reproducible processing pipeline rather than to optimize classification performance. Real-time clinical and VR-integrated EEG systems would require additional artifact-mitigation strategies, which are identified as future work.

3.4. Spatial Filtering and Referencing

EEG signals were analyzed using the native linked-ear reference provided in the PhysioNet dataset. No spatial filtering or re-referencing was applied: specifically, CAR, Laplacian (current source density) filtering, and CSP decomposition were not used. No CSP filter was applied in the original analysis. This limits claims concerning optimized post-cue decoding but does not explain the absence of pre-cue left–right differences.

3.5. Pre-Cue Window Extraction

EEG was segmented relative to the dataset task annotation. T0 denotes rest, while T1 and T2 denote the left and right target intervals. Because the recordings do not include independently measured movement-onset markers, the analyzed windows are defined relative to the annotation rather than actual movement. The interval from −1.0 to 0.0 s is the final

second before the task annotation, while −2.0 to −1.0 s is an earlier pre-annotation interval. These windows were fixed in advance and were not selected according to condition.

The same temporal boundaries and channel montage were applied identically to all conditions: rest, left-hand motor execution, right-hand motor execution, motor imagery, and combined motor-versus-rest contrasts. Condition labels were assigned from dataset annotations without condition-specific window tuning or data-driven optimization. The one-second analysis window also provides sufficient data for Welch PSD estimation.

3.6. Spectral Feature Modeling

To characterize neural activity within the pre-cue window, spectral features were extracted using Welch's method for PSD estimation. Analysis focused on the alpha band (8–12 Hz) and beta band (13–30 Hz), which are strongly associated with motor-related cortical activity.

Welch PSD estimation was performed using sciPy signal.welch function with a sampling frequency of $f_s = 160$ Hz. For the primary pre-cue window (−1.0 to 0.0 s), the epoch length was 160 samples; therefore, `nperseg` = 160 and `noverlap` = 80 (50% overlap) were used. A Hann window and constant detrending were applied using the SciPy default implementation. The fast Fourier transform (FFT) length was not explicitly specified and therefore followed the SciPy default behavior. Because the segment length equals the epoch length, each estimate is a single Hann-windowed periodogram. The specified overlap does not create additional segments and does not produce the variance reduction associated with averaging multiple Welch segments. Frequency-bin spacing is 1 Hz. Band power was integrated over alpha (8–12 Hz), SMR (12–15 Hz), beta (13–30 Hz), and high-beta (20–30 Hz). This setting matches the spectral window to the one-second epoch rather than implementing multi-segment Welch averaging. A supplementary 107-participant multitaper analysis (time-half-bandwidth 2.5; four tapers) preserved the direction of the principal raw-power decreases. Execution effect sizes were $d_z = -0.272$ (multitaper) versus −0.362 (Welch) for alpha and $d_z = -0.477$ versus −0.558 for beta. That sensitivity analysis does not replace the original 109-participant Kruskal–Wallis results ($H_\alpha = 74.79$; $H_\beta = 289.01$).

The computed spectral power values were extracted from the Welch PSD estimates and subject-wise normalized prior to statistical analysis. This transformation improves statistical stability and enables more reliable comparison across conditions. Additional derived features included relative band power and ERD measures, providing a comprehensive representation of neural activity within the pre-cue interval.

Beyond absolute alpha and beta band power, the feature set included: (i) relative band power (condition band power normalized by total power in the analysis window); and (ii) ERD/ERS, computed as percentage change in alpha power relative to the baseline window (−2.0 to −1.0 s). Sub-band analyses further examined sensorimotor rhythm (SMR, 12–15 Hz) and high-beta (HBeta, 20–30 Hz) components; HBeta exhibited the largest Rest-versus-Motor effect sizes ($|d| \approx 0.235$) in the pre-cue interval.

Alpha-band ERD/ERS was computed using the standard percentage-change formula [26]:

$$\text{ERD/ERS}\,(\%) = 100 \times \frac{P_{\text{pre}} - P_{\text{base}}}{P_{\text{base}}} \tag{1}$$

where P_{base} denotes integrated α power (8–12 Hz) in the baseline window (−2.0 to −1.0 s) and P_{pre} denotes integrated α power in the pre-cue window (−1.0 to 0.0 s), estimated via Welch PSD for each sensorimotor electrode. Negative values indicate ERD; positive values indicate ERS. Montage-mean values were computed across the thirteen electrodes prior to subject-wise normalization.

Beta-band modulation was defined as the change in beta-frequency spectral power (13–30 Hz) between the pre-cue and baseline windows, quantified through absolute band

power and relative band power (beta power normalized by total power in 1–40 Hz within each window). Beta modulation was assessed at the group level as condition-dependent differences in pre-cue beta power (Kruskal–Wallis). The historical one-sample *t*-tests compared condition epochs with the pooled Rest-condition mean in the same −1.0 to 0.0 s window, not with the temporal baseline. These tests are not retained as current inferential support.

3.7. Signal Variability and Noise Considerations

EEG signals inherently exhibit variability and are affected by measurement noise, particularly when analyzing low-amplitude neural activity. Signals within the pre-cue interval are typically close to the noise floor, making their detection challenging.

Variability arises from multiple sources, including inter-subject differences, background neural fluctuations, and recording conditions. To account for these factors, subject-wise normalization was applied to reduce inter-subject variability and improve comparability of feature values. No supplementary ICA- or threshold-based artifact rejection was applied beyond the controlled PhysioNet acquisition protocol. Subject-wise normalization attenuates inter-subject amplitude differences but does not constitute artifact rejection.

Signal quality was ensured through: (i) the use of controlled laboratory PhysioNet recordings; (ii) short temporal windows aligned to the dataset-annotated movement or imagery onset (−2.0 to 0.0 s); (iii) constant detrending and subject-wise normalization; and (iv) convergent statistical validation (bootstrap CIs, permutation testing, LMM, and FDR correction).

By considering realistic signal variability rather than synthetic noise injection, the analysis reflects practical conditions encountered in real-world neurorehabilitation systems.

3.8. Statistical Neural Signal Detection Framework

Detection of labeled-condition spectral differences was performed using a statistical analysis framework. In this study, detection is defined as the presence of statistically significant differences between baseline and motor-related conditions. Non-parametric group comparisons were conducted using the Kruskal–Wallis test due to the non-normal distribution of EEG features. Pairwise comparisons were performed using Dunn's post hoc test with Bonferroni correction. The original analysis also computed one-sample *t*-tests of condition epochs against the pooled Rest-condition mean in the same −1.0 to 0.0 s window. Those tests are retained only as a historical record of the implemented pipeline. They are not used as inferential support for H2, and they do not compare each condition with the −2.0 to −1.0 s temporal baseline used for ERD/ERS. To account for multiple comparisons, FDR correction using the Benjamini–Hochberg method was applied. In addition, Spearman rank correlation analysis was used to evaluate relationships between spectral features across conditions. The original Kruskal–Wallis, Dunn, bootstrap, and permutation analyses treated epochs as independent observational units ($N = 18{,}926$ from 109 participants). Those procedures did not account for within-subject dependence and are interpreted as historical epoch-level statistics rather than participant-level inference. The MixedLM specifies a participant random intercept but does not retrospectively correct the epoch-level nonparametric tests. Additional participant-level inference uses the 109 within-subject Motor-minus-Rest mean differences.

Temporal boundaries for ERD/ERS analysis were defined a priori rather than through data-driven change-point detection. The baseline window (−2.0 to −1.0 s) and pre-cue window (−1.0 to 0.0 s) were fixed uniformly across all conditions based on motor preparation neurophysiology (Section 3.3). ERD/ERS values were computed per epoch and aggregated for group-level testing via Kruskal–Wallis analysis (H1, Table 3), Dunn post hoc pairwise

comparisons with Bonferroni correction, mean-difference permutation testing (Motor vs. Rest), and Benjamini–Hochberg FDR correction. Non-parametric methods were selected due to confirmed non-normality of ERD/ERS distributions (Shapiro–Wilk test).

Table 3 maps each statistical procedure to its corresponding hypothesis. H1: pre-cue alpha power differs across rest and motor conditions (Kruskal–Wallis, Dunn post hoc). H2: The implemented one-sample comparison of condition epochs with the pooled Rest-condition mean in the same -1.0 to 0.0 s window was retained for documentation only and is not used as current inferential support. H3: Spectral co-variation of alpha and beta band power (Spearman), not conventional cross-frequency coupling. H4: Motor and imagery conditions show significant population-level fixed effects after controlling for subject variability (LMM). Permutation and bootstrap analysis test the null hypothesis that observed separability arises from chance.

Table 3. Mapping of statistical hypotheses, analytical methods, and decision criteria.

Hypothesis	Statistical Test	Decision Criterion
H1: α-band differences across conditions	Kruskal–Wallis test; Dunn post hoc comparisons (Bonferroni corrected)	Significant between-condition difference ($p < 0.05$ after correction)
H2: condition epochs versus the pooled Rest-condition mean in the same -1.0 to 0.0 s window	Historical one-sample t-test (not retained as inferential support)	Recorded for pipeline completeness only; not used to claim deviation from the -2.0 to -1.0 s temporal baseline
H3: spectral co-variation of α and β band power	Spearman rank correlation of band-power features	Rank association ($p < 0.05$); not phase–amplitude coupling, phase locking, or another conventional CFC estimator
H4: Population-level motor effect	LMM	Significant fixed effect after accounting for subject variability ($p < 0.05$)
Null hypothesis: chance separability	Bootstrap CIs; permutation testing	95% CI excluding zero and/or permutation significance ($p_{\text{perm}} < 0.05$)

This statistical framework evaluates whether labeled-condition spectral features differ from the annotated rest class.

3.9. Performance Evaluation Metrics

Detection performance was quantified using statistical measures rather than classification accuracy. The primary evaluation criterion was statistical significance, represented by p-values obtained from the applied tests.

To assess robustness, the consistency of significant results across multiple statistical tests was examined. FDR correction was used to ensure that significant findings were not due to multiple comparison effects.

Bootstrap CIs were computed to evaluate the stability of feature estimates across repeated resampling. These intervals provide an additional measure of reliability for the observed neural signal differences.

Together, these metrics provide a quantitative characterization of labeled-condition spectral differences under realistic conditions.

3.10. Computational Framework

A computational analysis framework was developed to evaluate annotation-locked labeled-condition spectral differences. EEG recordings from the PhysioNet dataset were used directly without synthetic signal generation.

The analysis included multiple conditions, including rest, motor execution, and motor imagery. For each condition, spectral features were extracted and statistically evaluated within the defined pre-cue window.

The framework systematically compares baseline and motor-related neural activity across subjects and conditions, providing a comprehensive evaluation of signal detectability in realistic scenarios. As illustrated in Figures 2 and 3, the framework integrates four implemented stages—(1) physiological EEG acquisition, (2) epoch extraction relative to the task annotation, (3) spectral feature modeling, and (4) multi-method statistical comparison.

3.11. Dataset and Labeling Strategy

EEG recordings were labeled according to task annotations provided in the dataset. Rest conditions were considered baseline neural activity, while motor execution and motor imagery conditions were treated as neural activation states. Segments corresponding to pre-cue intervals were extracted and associated with their respective task labels. This labeling strategy enables direct comparison between baseline and pre-cue neural activity. The same temporal boundaries (-2.0 to -1.0 s baseline; -1.0 to 0.0 s pre-cue) and sensorimotor electrode montage were applied uniformly across all experimental conditions, including rest, left-hand motor execution, right-hand motor execution, motor imagery, and motor-versus-rest comparisons. Condition labels were assigned directly from dataset annotations without condition-specific temporal optimization or window tuning, ensuring methodological consistency and cross-condition comparability. The labeling approach enables analysis of annotation-locked spectral differences between labeled conditions. Because the pre-cue windows reflect the preceding blocks, these differences cannot be interpreted as demonstrated motor intention detection.

A supplementary cue-locked analysis used 107 participants after excluding S088 and S092 from the original 109-subject list. Windows were defined relative to T1/T2 onsets that were fully contained in rest before the cue and in the task after the cue. Spectral comparisons used the last pre-cue rest second versus the first post-cue task second. Subject-held-out classification evaluated post-cue versus pre-cue rest and left-versus-right hand identity, including models residualized for the previous hand. These supplementary results are reported separately from the original 109-participant labeled-condition analysis and do not replace it.

3.12. Reproducibility

To facilitate independent replication, Table 4 provides a consolidated summary of the dataset, preprocessing, spectral estimation, statistical analysis, spatial processing, and code-availability settings used in this study.

Table 4. Reproducibility and analysis settings.

Item	Specification
Dataset	PhysioNet EEG Motor Movement/Imagery Database v1.0.0 (https://physionet.org/content/eegmmidb/1.0.0/ (accessed on 6 May 2026))
Subjects	All 109 available subjects; no exclusion.
Channels	C3, C1, Cz, C2, C4, CP1, CP3, CPz, CP2, CP4, FC1, FC2, and FCz.
Temporal windows	Baseline: -2.0 to -1.0 s; pre-cue: -1.0 to 0.0 s. Both were defined relative to the dataset task annotation ($t = 0$ s at T1/T2).
Welch parameters	$f_s = 160$ Hz, `nperseg` = 160, `noverlap` = 80, Hann window, constant detrend, with `nfft` left unspecified and therefore determined by the default SciPy (version 1.14.1) implementation. One 160-sample segment per epoch: a single Hann-windowed periodogram, 1 Hz bin spacing.

Table 4. *Cont.*

Item	Specification
Normalization	Subject-wise normalization.
Statistical tests	Kruskal–Wallis, Dunn post hoc (Bonferroni), one-sample t-tests (FDR), Spearman correlation, bootstrap CI (2000 resamples), mean-difference permutation testing (Motor vs. Rest), and LMM.
Spatial processing	Native linked-ear reference retained; no CAR, Laplacian, or CSP applied.
Artifact handling	No ICA-based rejection; subject-wise normalization only.
ERD/ERS analysis	Alpha ERD/ERS computation (Equation (1)), beta-band modulation definitions, and ERD/ERS statistical procedures are included in the replication checklist above.
Code availability	Analysis scripts implemented in Python 3.11, using SciPy 1.14.1, NumPy 2.1.3, and pandas 2.2.3, are available from the corresponding author upon reasonable request.

4. Results

We first examine the overall statistical differences, then the pairwise comparisons, followed by additional validation analyses and the physiological interpretation of the findings. Interpretive content was intentionally minimized within figures and is discussed in the corresponding captions and Results text to improve readability and conform to standard journal figure conventions.

4.1. Preceding-Block Identity of the Original −1 to 0 s Window

Preceding-block analysis showed that all 9781 aligned Left/Right epochs were preceded by rest, whereas all 9143 aligned Rest epochs were preceded by a task. Of 18,926 epochs, 18,924 were aligned successfully. Because preceding-block identity and upcoming-condition label are perfectly dependent, their contributions cannot be distinguished. The original Motor-minus-Rest difference therefore represents late rest minus late task. Subject-level paired differences were $+0.076$ alpha z units (95% CI 0.030–0.122; $p = 0.00132$) and $+0.204$ beta z units (95% CI 0.157–0.250; $p = 4.01 \times 10^{-14}$). These differences do not establish pre-movement activity associated with the upcoming trial. The original Kruskal–Wallis, Dunn, bootstrap, and permutation p-values treat epochs as independent ($N = 18{,}926$) and should not be read as participant-level inference. The MixedLM random-intercept variance for the subject-wise z-scored features was zero, consistent with subject-wise centering, and does not correct those epoch-level tests. The same 109-participant Motor-minus-Rest differences were $+0.07627$ for alpha z (Wilcoxon $p = 0.00218$; sign-flip $p = 0.00180$) and $+0.20371$ for beta z (Wilcoxon $p = 3.03 \times 10^{-12}$; sign-flip $p = 9.999 \times 10^{-5}$). Alpha ERD was nonsignificant by paired t (-6.22%; 95% CI -15.43 to $+2.99$; $p = 0.183$). Beta ERD was nonsignificant by paired t (-3.12%; 95% CI -7.02 to $+0.78$; $p = 0.116$) although Wilcoxon differed ($p = 0.00124$). These paired tests are not replacements for the original three-group Kruskal–Wallis or Dunn analyses.

4.2. Statistical Separability of Annotated Rest and Motor Labels

Figure 6 presents the results of the Kruskal–Wallis analysis for subject-normalized spectral features across rest, left, and right motor conditions ($N = 18{,}926$ epochs from 109 subjects). In the original labeling, alpha and beta power differed across the annotated conditions. This contrast compares the end of rest with the end of the preceding task, not a measured pre-movement interval with rest.

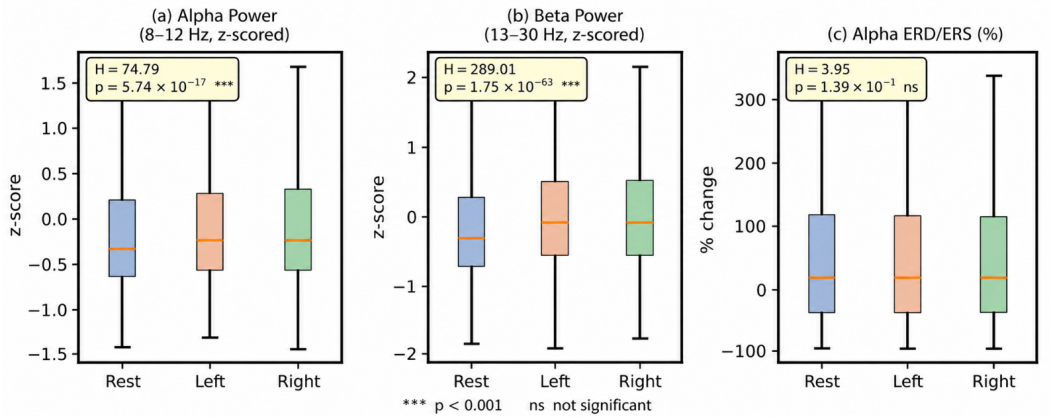


Figure 6. Kruskal–Wallis analysis of subject-normalized spectral features across rest, left, and right motor conditions ($N = 18{,}926$ epochs). Beta power ($H = 289.01$, $p \ll 0.001$) shows stronger separability than alpha power ($H = 74.79$, $p \ll 0.001$). Alpha ERD/ERS (%) is non-significant across conditions ($H = 3.95$, $p = 0.139$) under the Methods-faithful per-trial formula. The symbol *** indicates $p < 0.001$, whereas ns indicates a non-significant result.

As shown in Figure 6, beta band power demonstrated the strongest separability across conditions, with substantially higher test statistics ($H = 289.01$, $p = 1.75 \times 10^{-63}$) compared to alpha features ($H = 74.79$, $p = 5.74 \times 10^{-17}$). Alpha ERD/ERS (%) did not exhibit significant Kruskal–Wallis variation ($H = 3.95$, $p = 0.139$); the previously reported significant ERD claim is therefore not supported under the Methods-faithful per-trial ERD/ERS definition.

The original Motor-minus-Rest elevation in alpha and beta power is not evidence of pre-movement event-related desynchronization because the comparison represents late rest versus late task. In the supplementary cue-locked analysis of 107 participants, alpha and beta power decreased after the task annotation. Relative to the final pre-cue rest second, execution beta decreased by 15.0% and imagery beta by 12.1%. These changes are interpreted as cue-related spectral effects rather than verified movement-locked intention signals. In the same 107-participant cue-locked analysis, a contralateral-negative slow potential appeared after the cue (execution -8.32 µV from 0.3 to 0.8 s). This supplementary sample is distinct from the original 109-participant analysis.

Figure 7 shows subject-level Motor−Rest differences of the same primary z-scored alpha and beta features ($N = 109$ subjects; one aggregated value per subject). This supporting visualization does not replace the epoch-level Kruskal–Wallis, Dunn, MixedLM, or FDR results and does not change their numerical outcomes.

4.3. Pairwise Condition Differences and Post-Hoc Analysis

Figure 8 presents the results of the Dunn post hoc analysis with Bonferroni correction, visualized using pairwise comparison matrices across rest, left, and right motor conditions. As shown in Figure 8, statistically significant differences were consistently observed between the resting state and both motor-related conditions in alpha power and beta power (Bonferroni-corrected Dunn $p \ll 0.001$). Alpha ERD/ERS pairwise contrasts were non-significant (Rest–Left $p = 0.380$; Rest–Right $p = 0.255$; Left–Right $p = 1.000$).

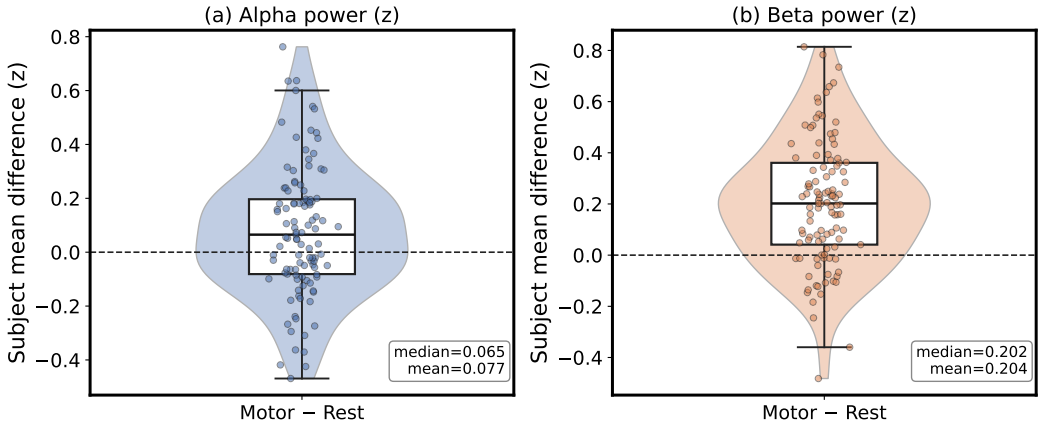


Figure 7. Supporting subject-level variability of Motor−Rest differences for primary alpha and beta z-scored power ($N = 109$). Each point is one subject after within-subject averaging of Rest and Motor (Left/Right) epochs. Population-level statistical tests remain those reported in Results; Alpha ERD/ERS is not presented as a supported primary finding.

Specifically, for alpha and beta power both left and right motor conditions differ significantly from rest ($p < 0.001$), while left–right comparisons remain non-significant. Alpha ERD/ERS shows no significant pairwise Rest-versus-Motor differences. This pattern, illustrated in Figure 8, reflects labeled-condition spectral separability driven by the contrast between late rest and late task, rather than independently verified motor activation or pre-movement intention. Left–right comparisons remain non-significant.

Left- and right-hand motor imagery and execution conditions were distinguished using PhysioNet task labels (visual target on left vs. right side of screen). The upcoming hand is indicated only when T1 or T2 begins. Supplementary pre-cue classification was at chance (montage-mean AUC 0.501). After controlling for previous-hand effects, C3/C4, FBCSP, and log-Euclidean models yielded execution AUCs of 0.491, 0.481, and 0.480, respectively. Post-cue hand classification yielded AUCs of 0.571 during execution and 0.594 during imagery. These post-cue values describe cue-locked left–right separation in the 107-participant supplementary analysis and do not establish pre-movement intention detection. The pre-cue null finding is therefore interpreted in relation to task timing and previous-trial structure rather than the absence of CSP alone. Dunn post hoc tests used Bonferroni correction, which controls the family-wise error rate among the pairwise contrasts.

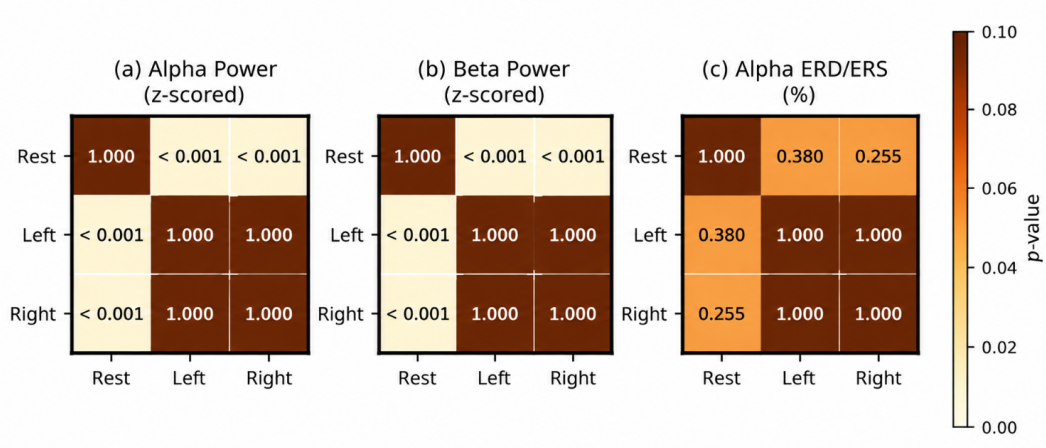


Figure 8. Dunn post hoc pairwise comparisons with Bonferroni correction across rest, left, and right conditions for alpha power, beta power, and alpha ERD/ERS. Rest-versus-motor contrasts are significant for alpha and beta power; alpha ERD/ERS contrasts are non-significant. Left–right differences remain non-significant for all three features.

4.4. Statistical Detectability of Labeled-Condition Spectral Differences

Figure 9 presents a multi-metric statistical summary of the original epoch-level Rest-versus-Motor comparison. No single scalar detectability index was calculated. The panel reports Kruskal–Wallis H, absolute Cohen's d, and permutation significance as separate quantities.

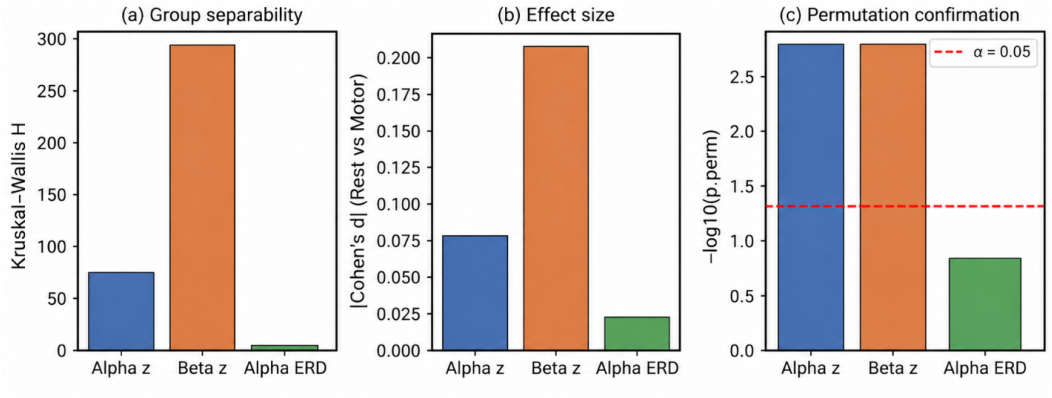


Figure 9. Multi-metric statistical summary of the original epoch-level Rest-versus-Motor comparison. Displayed quantities are Kruskal–Wallis H ($H_\alpha = 74.79$, $H_\beta = 289.01$), absolute Cohen's d ($|d|_\alpha \approx 0.077$, $|d|_\beta \approx 0.207$), and permutation significance at the 500-shuffle resolution floor of approximately 0.002. The red dashed line in panel (**c**) indicates the statistical significance threshold corresponding to $\alpha = 0.05$. These measures are not a composite detectability index and do not quantify single-trial intention detection.

Specifically, beta-band features exhibit higher detectability values than alpha features across all motor-related conditions, indicating stronger and more consistent condition-related signal expression within the analyzed pre-cue interval. Although the observed effect sizes remain within a low-to-moderate range (Rest-versus-Motor $|d|_\alpha \approx 0.077$, $|d|_\beta \approx 0.207$; alpha ERD $|d| \approx 0.021$), the large epoch sample (N = 18,926) inflates epoch-level power and does not constitute participant-level confirmation.

Figure 9 presents complementary epoch-level measures of the same labeled-condition contrast, including Kruskal–Wallis H, $|d|$, and permutation significance. These measures are not independent participant-level confirmations. The historical epoch-level bootstrap confidence intervals are descriptive and do not account for repeated observations within participants.

Overall, the results show differences in EEG spectral power across annotation-locked intervals. These findings support further investigation of sensorimotor EEG activity and its potential applications in future neurorehabilitation research.

4.5. Robustness Analysis Using Bootstrap CIs

Figure 10 presents bootstrap-derived 95% CIs for spectral EEG features across all experimental conditions, based on 2000 resampling iterations. Those original 2000 resamples were drawn at the epoch level: Rest, Left, Right, Imagery, and Execution observations were resampled independently, without preserving participant clusters. The displayed intervals therefore do not account for within-subject dependence. As shown in Figure 10, for alpha and beta power the CIs associated with Left and Right do not overlap the Rest interval. Alpha ERD/ERS (%) intervals overlap across conditions.

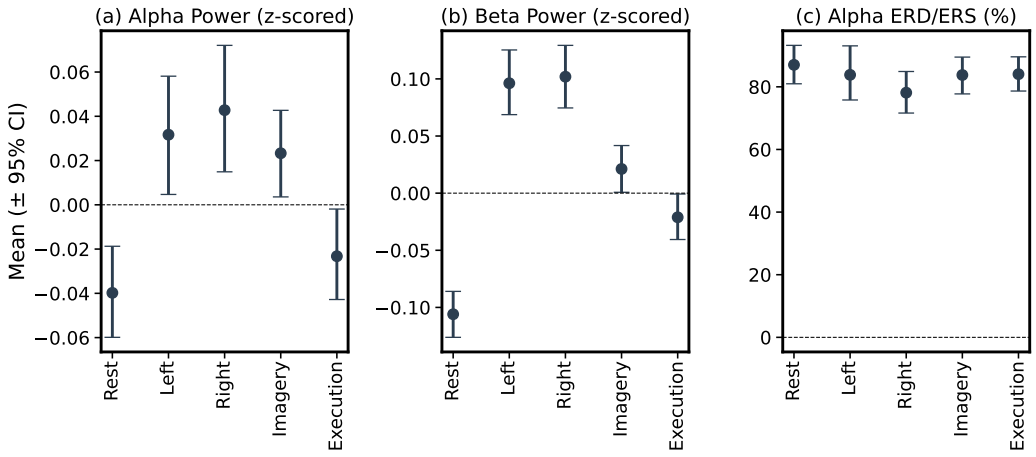


Figure 10. Original 2000-resample epoch-level bootstrap 95% CIs for Rest, Left, Right, Imagery, and Execution. Epochs were resampled independently within each label. Group sizes were Rest 9144, Left 4917, Right 4865, Imagery 9449, and Execution 9477. These intervals are a historical epoch-level display and are not interchangeable with participant-cluster or paired participant intervals.

A supplementary subject-cluster bootstrap used 2000 resamples of all 109 participants, drawing complete participant clusters while preserving the original epoch-weighted group-mean estimand (Table 5). Rest-versus-Left and Rest-versus-Right intervals remained non-overlapping for alpha and beta z-scored power; the corresponding alpha ERD intervals overlapped. The supplementary beta Imagery and Execution intervals included zero. Non-overlap of individual group-mean intervals is descriptive and does not replace a direct participant-aware test of the between-group difference. A separate paired participant bootstrap of Motor-minus-Rest differences yielded 95% intervals of $[0.0306, 0.1208]$ for alpha z, $[0.1580, 0.2523]$ for beta z, $[-14.97, 2.38]$ for alpha ERD, and $[-6.80, 1.04]$ for beta ERD. Those paired intervals address a different estimand from the group-mean intervals in Figure 10. None of these analyses is presented as pre-movement intention evidence.

Table 5. Supplementary subject-cluster bootstrap 95% CIs (2000 resamples of 109 participants; epoch-weighted group means). Historical epoch-level intervals from the original figure are shown for comparison. Source: PeerREV folder 14, seed 42.

Feature	Group	Epoch-Level 95% CI	Subject-Cluster 95% CI
Alpha z	Rest	$[-0.05989, -0.01873]$	$[-0.06249, -0.01633]$
Alpha z	Left	$[0.00468, 0.05812]$	$[0.00219, 0.05930]$
Alpha z	Right	$[0.01491, 0.07205]$	$[0.01387, 0.07201]$
Beta z	Rest	$[-0.12619, -0.08597]$	$[-0.13023, -0.08257]$
Beta z	Left	$[0.06872, 0.12532]$	$[0.06901, 0.12519]$
Beta z	Right	$[0.07458, 0.12934]$	$[0.07479, 0.12960]$
Beta z	Imagery	$[0.00075, 0.04167]$	$[-0.00149, 0.04355]$
Beta z	Execution	$[-0.04058, -0.00076]$	$[-0.04415, 0.00225]$

The original epoch-level intervals and the subject-cluster intervals in Table 5 are different estimands. Epoch-level Kruskal–Wallis, Dunn, bootstrap, permutation, and Shapiro–Wilk results do not independently establish participant-level robustness. Non-overlap of group-mean confidence intervals is descriptive and is not treated as proof of independently validated movement intention.

These bootstrap results describe labeled-condition spectral differences. They do not show that movement onset or motor intention was measured.

4.6. Distributional Characteristics and Justification of Non-Parametric Analysis

Figure 11 presents the results of the Shapiro–Wilk normality test applied to subject-normalized EEG spectral features across all experimental conditions. As shown in Figure 11, the majority of feature distributions have p-values below the significance threshold, indicating deviation from normality across both alpha and beta bands.

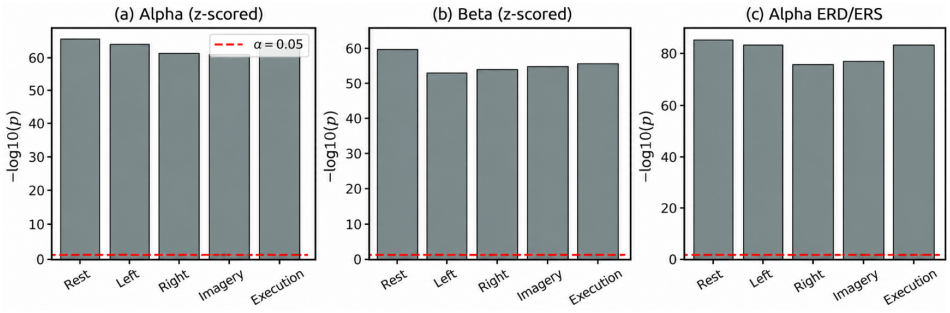


Figure 11. Shapiro–Wilk normality test results for EEG spectral features across conditions. Most distributions have p-values below the significance threshold, indicating deviation from normality and justifying the use of non-parametric statistical methods.

Non-normal distributions are consistently observed across rest, motor, imagery, and execution conditions, with particularly strong deviations in motor-related states. This distributional behavior reflects the inherent variability and skewness of EEG spectral features, especially within pre-cue temporal windows.

The observed non-normality directly justifies the use of non-parametric statistical methods, including the Kruskal–Wallis test and Dunn post hoc analysis, as adopted throughout this study. These methods do not rely on Gaussian assumptions and therefore provide a more appropriate framework for analyzing EEG data under realistic conditions.

Shapiro–Wilk results justify the original choice of non-parametric epoch-level tests. They do not correct within-subject dependence and do not independently validate participant-level inference.

Overall, these findings confirm that the non-parametric tests used for the labeled-condition contrast are appropriate under the observed non-Gaussian distributions.

4.7. Summary of Spectral Features in the Pre-Cue Window

Figure 12 summarizes the mean spectral characteristics of alpha and beta bands across all evaluated conditions. Clear differences are observed between resting and motor-related conditions, particularly in the beta band.

As shown in Figure 12, motor execution and motor imagery conditions exhibit increased beta power relative to rest, indicating condition-dependent beta modulation within the analyzed pre-cue interval. Alpha-band differences in this figure are labeled-condition spectral contrasts, not confirmed pre-movement ERD.

The distribution of epochs across conditions remains balanced (total $N = 18,926$: Rest 9144, Left 4917, Right 4865; Imagery 9449, Execution 9477), ensuring that statistical comparisons are not driven by extreme sample-size imbalance. This balanced representation strengthens the validity of the observed spectral differences across conditions.

The overall spectral trends are compatible with the neurophysiological patterns reported in the motor-preparation literature, including beta- and alpha-band modulation before annotated motor events.

These results provide a descriptive summary of the labeled-condition spectral differences. They do not establish independently timed pre-movement activity.

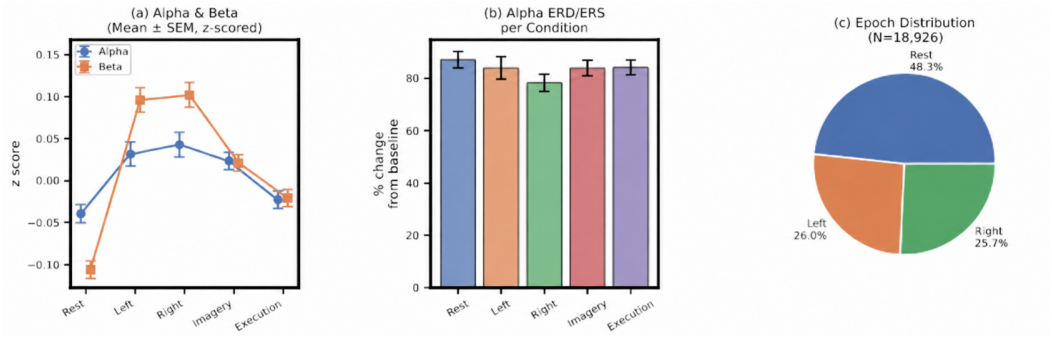


Figure 12. Mean spectral characteristics of alpha and beta bands across labeled rest, imagery, and execution conditions. The displayed differences are labeled-condition spectral contrasts. In the original 109-participant analysis this comparison is confounded with preceding-block identity (late rest versus late task) and is not confirmed pre-movement ERD or independently timed intention.

4.8. Temporal Evolution of Pre-Cue Neural Activity

Figure 13 illustrates the temporal progression of EEG features within the one-second interval preceding the dataset task annotation. Statistical separability increases as the analysis window approaches this annotated event.

As shown in Figure 13, alpha and beta detectability vary across sub-windows within the pre-cue interval (primary-window $H_\alpha = 74.79$, $H_\beta = 289.01$). Beta remains significant in all tested windows; alpha remains significant for windows of duration ≥ 0.5 s. These patterns are compatible with preparatory modulation but do not independently identify the precise onset of motor intention. The observed increase in statistical separability as the dataset-provided event annotation approached is compatible with previously reported motor-related anticipatory activity. These findings support the analytical usefulness of the -1.0 to 0.0 s pre-cue window but do not independently identify the precise onset of motor intention. Statistical separability increased as the analysis window approached the dataset-provided event annotation. This pattern indicates stronger detectability closer to the annotated event and may be consistent with anticipatory motor-related activity; however, it does not independently establish the precise onset of motor intention.

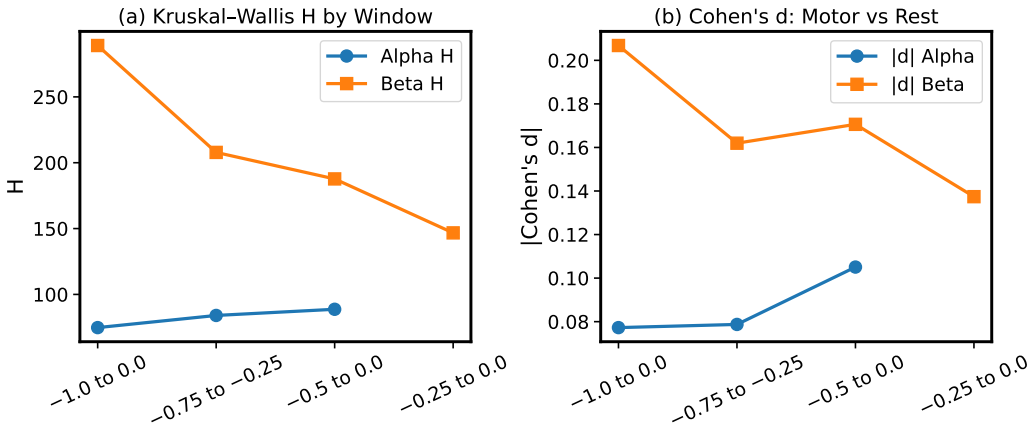


Figure 13. Temporal-window sweep of Kruskal–Wallis H and |Cohen's d| (Motor vs. Rest) for alpha and beta power across -1.0–0.0, -0.75–-0.25, -0.5–0.0, and -0.25–0.0 s. Beta separability remains significant in all windows; the shortest window cannot resolve the alpha band under Welch ($\geq$2 frequency bins), so alpha H is undefined there.

4.9. Validation Using Mean-Difference Permutation Testing

Figure 14 presents the results of mean-difference permutation testing (Motor vs. Rest). Permutation tests using 500 shuffles have a minimum attainable p-value of $1/501 \approx 0.0020$.

The alpha and beta z-score differences reached this resolution floor. Repetition with 10,000 shuffles yielded the corresponding floor of approximately 9.999×10^{-5}. These values reflect the resolution of the permutation procedure and should not be interpreted as exact tail probabilities below the attainable threshold. Epoch-level permutation inference is distinguished from participant-level inference. Alpha ERD/ERS did not reach the floor ($p_{\text{perm}} = 0.142$ in the original 500-shuffle test).

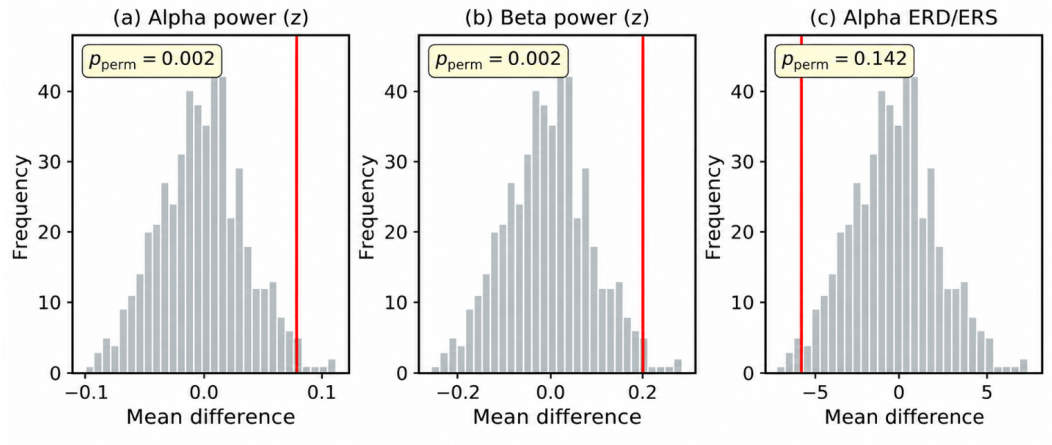


Figure 14. Mean-difference permutation tests (Motor vs. Rest; $n_{\text{perm}} = 500$). The minimum attainable p-value is $1/501 = 0.001996$. Alpha and beta z-score contrasts reached this floor; alpha ERD/ERS did not ($p_{\text{perm}} = 0.142$). The plotted $p \approx 0.002$ values are resolution-limited epoch-level results, not subject-level p-values.

4.10. Population-Level Analysis Using LMM

Figure 15 presents the results of the LMM, which explicitly accounts for subject-level variability through random effects.

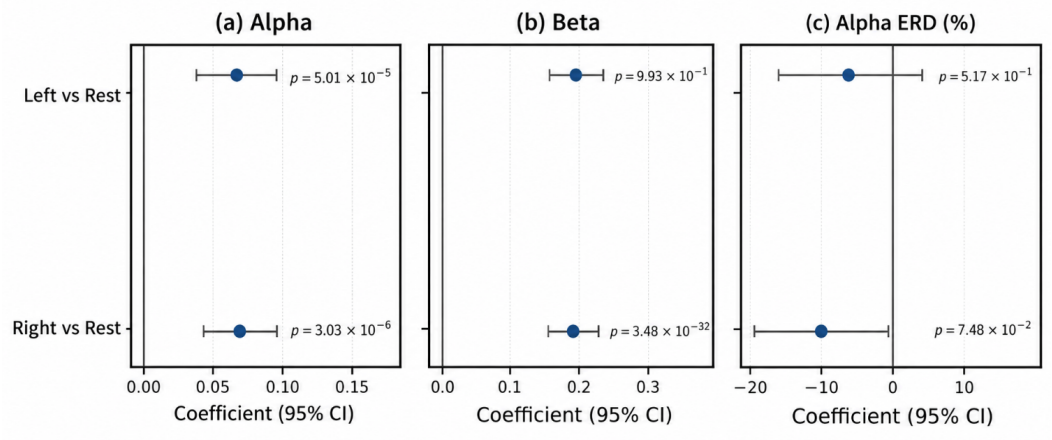


Figure 15. MixedLM fixed effects for Left and Right versus Rest (formula $y \sim C(\text{label_name}, \text{Treatment}(\text{reference} = \text{Rest}))$; random intercept per subject). Alpha and beta power show significant Left/Right effects; alpha ERD/ERS fixed effects are non-significant. Subject random-intercept variance is near zero for alpha/beta power.

As shown in Figure 15, significant Left and Right versus Rest fixed effects were observed for alpha power (Left coef $= 0.071$, $p = 5.0 \times 10^{-5}$; Right coef $= 0.083$, $p = 3.0 \times 10^{-6}$) and beta power (Left coef $= 0.202$, $p = 9.9 \times 10^{-31}$; Right coef $= 0.208$, $p = 3.5 \times 10^{-32}$). Alpha ERD/ERS fixed effects were insignificant (Left $p = 0.517$; Right $p = 0.075$).

The estimated random effect variance associated with subject intercepts is negligible. For the subject-wise z-scored features the MixedLM random-intercept variance was zero, which is consistent with subject-wise centering and does not retrospectively correct the epoch-level Kruskal–Wallis, Dunn, bootstrap, or permutation tests.

The MixedLM includes a participant-level random intercept, but its estimated variance was zero for the subject-wise standardized alpha and beta features. Consequently, these model results should be interpreted cautiously and do not establish independent validation of the epoch-level comparisons.

These results confirm population-level Left/Right versus Rest effects for alpha and beta power after accounting for subject intercepts; alpha ERD/ERS does not show significant MixedLM fixed effects.

4.11. Correction for Multiple Comparisons

Figure 16 presents the results of FDR correction using the Benjamini–Hochberg procedure applied across all statistical tests.

The historical Benjamini–Hochberg analysis rejected 14 of 21 tests at $q = 0.05$. That original family, defined in `fdr_bh.csv`, included twelve one-sample t-tests against the pooled Rest mean, and eight of those twelve t-tests were among the 14 rejections. The 14/21 count is therefore a historical record of the implemented pipeline. It is not used as independent confirmation of the revised findings, and the family was not recalculated after those t-tests were withdrawn as inferential support for H2. The remaining historical rejections were the Kruskal–Wallis and permutation contrasts for alpha and beta z and the Mann–Whitney imagery-versus-execution contrasts for alpha and beta z. Alpha-ERD family tests in that list were non-significant.

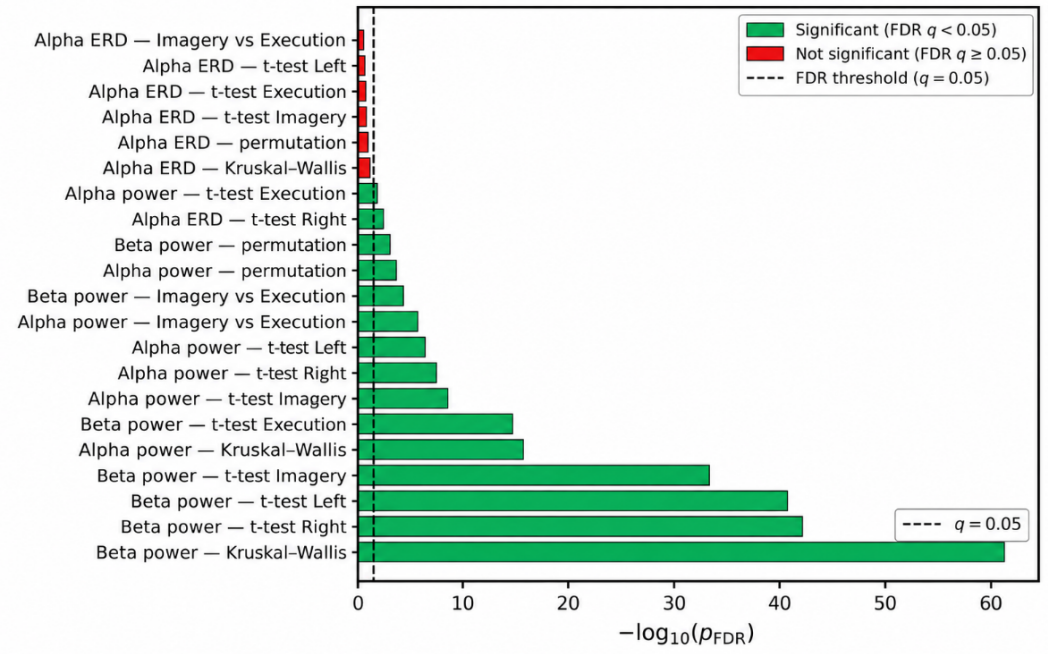


Figure 16. Historical Benjamini–Hochberg FDR display for the original 21-test family at $q = 0.05$ (14 rejections). That family included the one-sample t-tests withdrawn under H2. The 14/21 count is therefore a historical record of the original test family, not current independent inferential support. Benjamini–Hochberg controls the false discovery rate, not the family-wise error rate. Green bars indicate FDR-significant results, red bars indicate non-significant results, and the dashed vertical line marks the FDR significance threshold at $q = 0.05$.

4.12. Physiological Interpretation of the Labeled-Condition Contrast

Although alpha-band power differs across rest and motor conditions, the Methods-faithful per-trial alpha ERD/ERS metric is not significant at the group level; therefore we do not claim confirmed condition-dependent ERD as a primary result. In the original 109-participant analysis these alpha and beta differences compare late rest with late task. They are compatible with motor-related spectral modulation reported in the literature, but they are not independently timed pre-movement markers and do not demonstrate intention detection. The supplementary 107-participant findings are cue-locked: alpha and beta power decreased after the task annotation, and a contralateral slow potential appeared after the cue. Those results are separate from the original 109-participant labeled-condition contrast.

Sub-band analysis showed that HBeta (20–30 Hz) components exhibited the largest effect sizes ($|d| \approx 0.235$) in the original labeled window, while SMR (12–15 Hz) modulation was consistent with established motor-related neurophysiology [26,27]. High-beta is nested within beta and is not an independent biomarker.

4.13. Detectability Confirmation

Taken together, the analyses support Rest-versus-Motor spectral-power separability for alpha and beta power, whereas alpha ERD/ERS is not treated as a primary confirmed finding. Complementary checks for that labeled contrast include Dunn post hoc tests, bootstrap confidence intervals, permutation testing, and MixedLM with a subject random intercept. The historical Benjamini–Hochberg 14/21 result is not counted among those complementary checks. The statistical analyses provide complementary descriptions of labeled-condition spectral differences. However, the original Kruskal–Wallis, Dunn, bootstrap, and permutation analyses rely on repeated epochs and do not constitute independent participant-level confirmation. The supplementary participant-level paired analyses provide separate evidence for late-rest versus late-task differences, without establishing pre-movement intention detection. These findings characterize EEG spectral differences across annotated conditions and provide a methodological basis for future investigations of EEG-informed feedback in interactive neurorehabilitation environments. That future application remains conceptual. The present results establish statistical separability of annotated labels and cue-locked spectral change, not a working intention detector or VR system.

4.14. Feature Ranking and Biomarker Selection

Beyond individual hypothesis tests, we formalized a transparent feature-ranking/biomarker-selection layer over the verified spectral markers (alpha power, beta power, SMR, high-beta, alpha relative power, and alpha ERD/ERS). Categories were assigned by the original ranking procedure. Missing criteria were skipped rather than treated as failures. The Unsupported category is defined by a Kruskal–Wallis $p \geq 0.05$, with alpha ERD also assigned to this category. Primary requires a significant Kruskal–Wallis result, $|d| \geq 0.20$, and no failed evaluated permutation or MixedLM criterion. Secondary requires a significant Kruskal–Wallis result together with $|d| \geq 0.10$ or support from both evaluated permutation and MixedLM criteria. The Complementary category includes significant features that do not meet those thresholds. Beta z met six evaluated criteria; high-beta z was evaluated only for Kruskal–Wallis significance and effect size. High-beta (20–30 Hz) is nested within beta (13–30 Hz) and is not treated as an independent biomarker. The rankings describe exploratory labeled-condition separability, not validated pre-movement predictors.

Table 6 summarizes the feature-ranking results from the original verified outputs.

Table 6. Feature-ranking summary from the original verified outputs. Categories follow the explicit rules in the text. High-beta is a nested sub-band of beta and is not an independent biomarker.

Feature	H	p	$\lvert d \rvert$	Category
Beta power (z)	289.01	1.75×10^{-63}	0.207	Primary candidate
High-beta (20–30 Hz, z)	343.41	2.69×10^{-75}	0.235	Primary candidate
Alpha power (z)	74.79	5.74×10^{-17}	0.077	Secondary candidate
SMR (12–15 Hz, z)	143.78	6.00×10^{-32}	0.134	Secondary candidate
Alpha relative power	54.08	1.80×10^{-12}	–	Complementary feature
Alpha ERD/ERS (%)	3.95	0.139	0.021	Unsupported

Note: An en dash (–) indicates that Cohen's d was not reported for the corresponding feature.

Figure 17 illustrates the original feature-ranking results based on effect sizes and multi-criterion support.

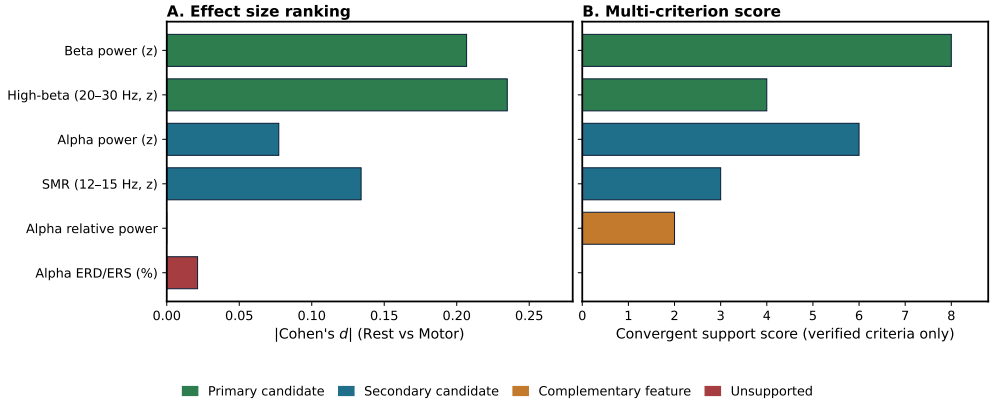


Figure 17. Original feature-ranking display of Rest-versus-Motor $|d|$ and multi-criterion support. Categories follow the Primary/Secondary/Complementary/Unsupported rules stated in the text. High-beta (20–30 Hz) is nested in beta (13–30 Hz) and is not an independent biomarker.

Under these rules, beta power and high-beta power emerge as primary candidates; alpha power and SMR as secondary candidates; alpha relative power as a complementary descriptor; and alpha ERD/ERS as unsupported. This separation is the operational output of the ranking layer and does not imply significance for non-significant markers.

4.15. Convergent Reliability Framework

The multi-method battery is interpreted as complementary checks for the labeled-condition contrast. Kruskal–Wallis, Dunn post hoc (Bonferroni family-wise error control), bootstrap confidence intervals, permutation testing, MixedLM, and Benjamini–Hochberg false-discovery-rate correction remain in the text. Benjamini–Hochberg correction controls the false discovery rate, whereas the Bonferroni correction used for Dunn's post hoc comparisons controls the family-wise error rate within the relevant comparison family.

SMR power (12–15 Hz) showed a statistically significant difference between the original labeled conditions (H = 143.78, $p = 6.00 \times 10^{-32}$), suggesting its potential relevance as an exploratory feature for understanding sensorimotor EEG activity. However, further investigation is needed to establish its relationship with movement onset and pre-movement intention.

5. Discussion

5.1. Interpretation of the Labeled-Condition Contrast

The original 109-subject analysis shows that the labeled conditions differ in alpha and beta power ($N = 18{,}926$; $H_\alpha = 74.79$; $H_\beta = 289.01$). That difference is late rest

versus late task. Methods-faithful alpha ERD/ERS is insignificant. Small Cohen's d values (Rest-versus-Motor $|d|_{\alpha} \approx 0.077$, $|d|_{\beta} \approx 0.207$) describe that labeled contrast.

Blankertz et al. [20] and Schalk et al. [32] are methodological and software references, respectively, rather than pre-movement detection benchmarks. Movement-intention studies that lock to electromyography or self-paced onset [36–43] address a different alignment event than the present cue-locked files. The unsupported 70–85% accuracy comparison has been removed, as have statements that attributed verified 0.5–1.0 s pre-movement timing to references [31,32]. Supplementary single-trial analyses do not establish intention detection: post-cue task-versus-rest classification yielded an AUC of 0.595, and pre-cue hand classification fell to chance after control for the previous trial.

The present findings contribute to the characterization of sensorimotor EEG activity and offer a methodological foundation for future neurorehabilitation research. Translation into interactive rehabilitation environments would benefit from additional movement-onset measurements, real-time validation, and evaluation in relevant clinical populations. Table 1 compares designs, alignment events, and movement measurements only.

Because Methods-faithful alpha ERD/ERS is insignificant at the group level, we interpret alpha findings primarily through power (z-scored) contrasts rather than as confirmed ERD magnitude effects.

5.2. Exploratory Feature Ranking

The following table summarizes the original ranking of spectral features. Recommended roles are future-work suggestions only.

Several considerations should be taken into account when interpreting the present findings. First, the study was conducted using offline analyses of a publicly available EEG dataset. Accordingly, the potential application of these findings to real-time EEG-informed rehabilitation warrants further investigation in interactive and clinical settings. Second, the available task annotations provide a useful temporal reference for examining EEG activity in relation to motor tasks, while more precise temporal characterization could further strengthen the interpretation of movement-related neural dynamics. Table 7 summarizes the exploratory spectral features and their potential relevance to future EEG-based neurorehabilitation research.

Table 7. Exploratory summary of spectral features and their potential relevance to future EEG-based neurorehabilitation research.

Feature	Effect Strength	Category	Potential Future Research Relevance
Beta power (z)	Stronger (within study)	Primary candidate	Candidate spectral feature for further evaluation in future EEG-informed neurorehabilitation feedback research
High-beta (20–30 Hz, z)	Stronger (within study)	Primary candidate	Candidate spectral feature for further evaluation in future EEG-informed neurorehabilitation feedback research
Alpha power (z)	Small	Secondary candidate	Secondary/supporting detectability cue; useful in multi-feature evidence rules
SMR (12–15 Hz, z)	Moderate-low	Secondary candidate	Secondary/supporting detectability cue; useful in multi-feature evidence rules
Alpha relative power	KW-significant (Cohen's d not reported)	Complementary feature	Complementary descriptor; not a standalone control biomarker in this study
Alpha ERD/ERS (%)	Negligible/non-significant	Unsupported	Not recommended as a primary control feature under current pipeline

The original −1 to 0 s comparison may also reflect differences associated with preceding task blocks, which should be considered when interpreting pre-cue spectral activity. Third, although supplementary participant-level analyses provide additional evidence

regarding the Motor-versus-Rest comparison, future studies could benefit from statistical approaches that more comprehensively account for repeated observations and comparisons across conditions. Finally, the supplementary pre-cue classification analysis highlights opportunities for further refinement of EEG-based prediction approaches, particularly through individualized modeling and more detailed investigation of sensorimotor dynamics. Overall, the observed sensorimotor EEG characteristics may provide a basis for future investigations of personalized feedback strategies, including potential applications in VR-based neurorehabilitation. Nevertheless, the PhysioNet EEG Motor Movement/Imagery dataset provides a reproducible basis for investigating EEG activity across motor execution and imagery conditions. The primary contribution of this study is the analysis of annotation-locked alpha- and beta-band spectral differences using complementary statistical methods. The findings describe differences between preceding rest and task intervals and highlight the importance of temporal alignment when interpreting motor-related EEG activity. These findings may provide a basis for future research exploring the use of EEG spectral features in VR-based neurorehabilitation. This approach is consistent with previous EEG and BCI studies that have used established public datasets to investigate neural activity through different analytical methods [14,15,17,21].

In summary, the original 109-participant analysis shows labeled-condition spectral differences that correspond to late rest versus late task. The supplementary 107-participant analysis shows cue-locked spectral and slow-potential effects. Neither analysis demonstrates independently measured movement onset or reliable pre-movement intention detection.

6. Conclusions

The original 109-subject analysis shows labeled-condition differences in alpha and beta power ($N = 18{,}926$; $H_\alpha = 74.79$; $H_\beta = 289.01$). Alpha ERD/ERS is non-significant ($H = 3.95$, $p = 0.139$). This study examined alpha- and beta-band power in EEG recordings of motor execution and motor imagery using spectral and statistical analyses. Significant differences were observed across annotated conditions, although their interpretation depended on the timing of the task annotations. The results provide a basis for further studies of EEG-based feedback and its potential use in future neurorehabilitation applications.

Author Contributions: Conceptualization, A.R. and Y.C.; methodology, A.R. and Y.C.; software, A.R.; validation, A.R.; formal analysis, A.R.; investigation, A.R.; resources, A.R.; data curation, A.R.; writing—original draft preparation, A.R.; writing—review and editing, A.R. and Y.C.; visualization, A.R.; supervision, Y.C. All authors have read and agreed to the published version of the manuscript.

Funding: This research received no external funding.

Institutional Review Board Statement: Ethical review and approval were not sought for this study because it involved secondary analysis of publicly available, de-identified EEG recordings from the PhysioNet EEG Motor Movement/Imagery Database, with no new participant recruitment, intervention, or collection of identifiable personal information.

Informed Consent Statement: This study involved secondary analysis of publicly available, de-identified EEG recordings from the PhysioNet EEG Motor Movement/Imagery Database. No participants were recruited, and no new informed consent was obtained by the authors. Consent procedures for the original data collection were outside the scope of this secondary analysis.

Data Availability Statement: The EEG data used in this study were obtained from the publicly available PhysioNet EEG Motor Movement/Imagery dataset (https://physionet.org/content/eegmmidb/1.0.0/ (accessed on 6 May 2026)). Complete reproducibility information—including subject selection (all 109 subjects from the validated OK file list; primary-window $N = 18{,}926$ epochs), channel list (C3, C1, Cz, C2, C4, CP1, CP3, CPz, CP2, CP4, FC1, FC2, and FCz), temporal windows (baseline -2.0

to −1.0 s; pre-cue −1.0 to 0.0 s), Welch parameters ($f_s = 160$ Hz after resampling 18 native-128 Hz files, `nperseg` = 160, `noverlap` = 80, Hann, constant detrend; trapezoidal band integration), per-trial ERD/ERS without clipping or pooled baseline, subject-wise z-score normalization, MixedLM primary model, and statistical test specifications—is provided in Section 3 and the accompanying analysis repository. Processed data, analysis scripts (Python 3.11), and analysis outputs supporting the findings of this study are available from the corresponding author upon reasonable request.

Acknowledgments: The authors used standard signal processing and statistical analysis tools implemented in Python 3.11 for experimental analysis.

Conflicts of Interest: The authors declare no conflicts of interest.

References

1. Hao, J.; Crum, G.; Siu, K.-C. Effects of Virtual Reality on Stroke Rehabilitation: An Umbrella Review of Systematic Reviews. *Health Sci. Rep.* **2024**, *7*, e70082. [CrossRef] [PubMed]
2. Prajjwal, P.; Chandrasekar, K.K.; Battula, P.; Gaviria, E.; Awe, M.O.; Inban, P.; Almutairi, A.S.; Das, A.; Tekuru, Y.; Marsool, M.D.M.; et al. The Efficacy of Virtual Reality-Based Rehabilitation in Improving Motor Function in Patients with Stroke: A Systematic Review and Meta-Analysis. *Ann. Med. Surg.* **2024**, *86*, 5425–5438. [CrossRef] [PubMed]
3. Maier, M.; Ballester, B.R.; Verschure, P.F.M.J. Principles of Neurorehabilitation After Stroke Based on Motor Learning and Brain Plasticity Mechanisms. *Front. Syst. Neurosci.* **2019**, *13*, 74. [CrossRef] [PubMed]
4. Kleim, J.A.; Jones, T.A. Principles of Experience-Dependent Neural Plasticity: Implications for Rehabilitation After Brain Damage. *J. Speech Lang. Hear. Res.* **2008**, *51*, S225–S239. [CrossRef] [PubMed]
5. Peng, Q.; Yin, L.; Cao, Y. Effectiveness of Virtual Reality in the Rehabilitation of Motor Function of Patients with Subacute Stroke: A Meta-Analysis. *Front. Neurol.* **2021**, *12*, 639535. [CrossRef] [PubMed]
6. Proffitt, R.; Lange, B. Considerations in the Efficacy and Effectiveness of Virtual Reality Interventions for Stroke Rehabilitation: Moving the Field Forward. *Phys. Ther.* **2015**, *95*, 441–448. [CrossRef] [PubMed]
7. Laver, K.E.; Lange, B.; George, S.; Deutsch, J.E.; Saposnik, G.; Chapman, M.; Crotty, M. Virtual Reality for Stroke Rehabilitation. *Cochrane Database Syst. Rev.* **2025**, *2025*, CD008349. [CrossRef] [PubMed]
8. Krohn, M.; Rintala, A.; Immonen, J.; Sjögren, T. The Effectiveness of Therapeutic Exercise Interventions with Virtual Reality on Balance and Walking Among Persons with Chronic Stroke: Systematic Review, Meta-Analysis, and Meta-Regression of Randomized Controlled Trials. *J. Med. Internet Res.* **2024**, *26*, e59136. [CrossRef] [PubMed]
9. Sharma, D.A.; Chevidikunnan, M.F.; Khan, F.R.; Gaowgzeh, R.A. Effectiveness of Knowledge of Result and Knowledge of Performance in the Learning of a Skilled Motor Activity by Healthy Young Adults. *J. Phys. Ther. Sci.* **2016**, *28*, 1482–1486. [CrossRef] [PubMed]
10. Winstein, C.J. Knowledge of Results and Motor Learning—Implications for Physical Therapy. *Phys. Ther.* **1991**, *71*, 140–149. [CrossRef] [PubMed]
11. Rah, A.; Chen, Y. Virtual Reality as a Stress Measurement Platform: Real-Time Behavioral Analysis with Minimal Hardware. *Sensors* **2025**, *25*, 5323. [CrossRef] [PubMed]
12. Rah, A.; Chen, Y. Virtual Reality Centric Stress Detection Using Dynamic Baseline Calibration. *Electronics* **2025**, *14*, 4501. [CrossRef]
13. Rah, A.; Chen, Y. Stroke Rehabilitation in Virtual Reality Through Enhanced Plantar Pressure Detection Using Sensor Resolution and Adaptive Thresholding. *Algorithms* **2026**, *19*, 368. [CrossRef]
14. Wolpaw, J.R.; Birbaumer, N.; McFarland, D.J.; Pfurtscheller, G.; Vaughan, T.M. Brain–Computer Interfaces for Communication and Control. *Clin. Neurophysiol.* **2002**, *113*, 767–791. [CrossRef] [PubMed]
15. Lotte, F.; Bougrain, L.; Cichocki, A.; Clerc, M.; Congedo, M.; Rakotomamonjy, A.; Yger, F. A Review of Classification Algorithms for EEG-Based Brain–Computer Interfaces: A 10-Year Update. *J. Neural Eng.* **2018**, *15*, 031005. [CrossRef] [PubMed]
16. Vidal, J.J. Toward Direct Brain–Computer Communication. *Annu. Rev. Biophys. Bioeng.* **1973**, *2*, 157–180. [CrossRef] [PubMed]
17. Goldberger, A.L.; Amaral, L.A.N.; Glass, L.; Hausdorff, J.M.; Ivanov, P.C.; Mark, R.G.; Mietus, J.E.; Moody, G.B.; Peng, C.-K.; Stanley, H.E. PhysioBank, PhysioToolkit, and PhysioNet: Components of a New Research Resource for Complex Physiologic Signals. *Circulation* **2000**, *101*, e215–e220. [CrossRef] [PubMed]
18. Daly, J.J.; Wolpaw, J.R. Brain–Computer Interfaces in Neurological Rehabilitation. *Lancet Neurol.* **2008**, *7*, 1032–1043. [CrossRef] [PubMed]
19. Laver, K.E.; Lange, B.; George, S.; Deutsch, J.E.; Saposnik, G.; Crotty, M. Virtual Reality for Stroke Rehabilitation. *Cochrane Database Syst. Rev.* **2017**, *11*, CD008349. [CrossRef] [PubMed]
20. Blankertz, B.; Tomioka, R.; Lemm, S.; Kawanabe, M.; Müller, K.-R. Optimizing Spatial Filters for Robust EEG Single-Trial Analysis. *IEEE Signal Process. Mag.* **2008**, *25*, 41–56. [CrossRef]

21. McFarland, D.J.; Wolpaw, J.R. EEG-Based Brain–Computer Interfaces. *Curr. Opin. Biomed. Eng.* **2017**, *4*, 194–200. [CrossRef] [PubMed]
22. Aderinto, N.; Olatunji, G.; Abdulbasit, M.O.; Edun, M.; Aboderin, G.; Egbunu, E. Exploring the Efficacy of Virtual Reality-Based Rehabilitation in Stroke: A Narrative Review of Current Evidence. *Ann. Med.* **2023**, *55*, 2285907. [CrossRef] [PubMed]
23. Mani Bharathi, V.; Manimegalai, P.; George, S.T.; Pamela, D.; Mohammed, M.A.; Abdulkareem, K.H.; Jaber, M.M.; Damaševičius, R. A Systematic Review of Techniques and Clinical Evidence to Adopt Virtual Reality in Post-Stroke Upper Limb Rehabilitation. *Virtual Real.* **2024**, *28*, 172. [CrossRef]
24. Baníková, Š.; Najsrová, A.; Szegedi, I.; Vítová, K.; Fiedorová, I.; Trdá, J.; Volný, O. Patient Satisfaction and Tolerance of Virtual Reality Rehabilitation in Subacute Ischemic Stroke: A Pilot Study. *Front. Rehabil. Sci.* **2025**, *6*, 1660766. [CrossRef] [PubMed]
25. Grimm, F.; Naros, G.; Gharabaghi, A. Closed-Loop Task Difficulty Adaptation During Virtual Reality Reach-to-Grasp Training Assisted with an Exoskeleton for Stroke Rehabilitation. *Front. Neurosci.* **2016**, *10*, 518. [CrossRef] [PubMed]
26. Pfurtscheller, G.; Lopes da Silva, F.H. Event-Related EEG/MEG Synchronization and Desynchronization: Basic Principles. *Clin. Neurophysiol.* **1999**, *110*, 1842–1857. [CrossRef] [PubMed]
27. Pfurtscheller, G.; Neuper, C. Future Prospects of ERD/ERS in the Context of Brain–Computer Interface (BCI) Developments. *Prog. Brain Res.* **2006**, *159*, 433–437. [CrossRef] [PubMed]
28. Kornhuber, H.H.; Deecke, L. Hirnpotentialänderungen bei Willkürbewegungen und passiven Bewegungen des Menschen: Bereitschaftspotential und reafferente Potentiale. *Pflügers Arch.* **1965**, *284*, 1–17. [CrossRef]
29. Walter, W.G.; Cooper, R.; Aldridge, V.J.; McCallum, W.C.; Winter, A.L. Contingent Negative Variation: An Electric Sign of Sensori-Motor Association and Expectancy in the Human Brain. *Nature* **1964**, *203*, 380–384. [CrossRef] [PubMed]
30. Bozinovska, L.; Bozinovski, S.; Stojanov, G. Electroexpectogram: Experimental Design and Agorithms. In Proceedings of the 1992 International Biomedical Engineering Days, Istanbul, Turkey, 18–20 August 1992; pp. 55–60. [CrossRef]
31. Pfurtscheller, G.; Neuper, C. Motor Imagery Activates Primary Sensorimotor Area in Humans. *Neurosci. Lett.* **1997**, *239*, 65–68. [CrossRef] [PubMed]
32. Schalk, G.; McFarland, D.J.; Hinterberger, T.; Birbaumer, N.; Wolpaw, J.R. BCI2000: A General-Purpose Brain–Computer Interface (BCI) System. *IEEE Trans. Biomed. Eng.* **2004**, *51*, 1034–1043. [CrossRef] [PubMed]
33. Maris, E.; Oostenveld, R. Nonparametric Statistical Testing of EEG- and MEG-Data. *J. Neurosci. Methods* **2007**, *164*, 177–190. [CrossRef] [PubMed]
34. Rah, A.; Chen, Y. Electrodermal Temperature-Adjusted Electrodermal Activity (EDA) for Stress Detection in Virtual Reality. *Sensors* **2026**, *26*, 2983. [CrossRef] [PubMed]
35. Lang, C.E.; MacDonald, J.R.; Reisman, D.S.; Boyd, L.A.; Kimberley, T.J.; Schindler-Ivens, S.; Hornby, T.G.; Ross, S.A.; Scheets, P.L. Observation of Amounts of Movement Practice Provided During Stroke Rehabilitation. *Arch. Phys. Med. Rehabil.* **2009**, *90*, 1692–1698. [CrossRef] [PubMed]
36. Niazi, I.K.; Jiang, N.; Tiberghien, O.; Nielsen, J.F.; Dremstrup, K.; Farina, D. Detection of movement intention from single-trial movement-related cortical potentials. *J. Neural Eng.* **2011**, *8*, 066009. [CrossRef] [PubMed]
37. Bai, O.; Rathi, V.; Lin, P.; Huang, D.; Battapady, H.; Fei, D.-Y.; Schneider, L.; Houdayer, E.; Chen, X.; Hallett, M. Prediction of human voluntary movement before it occurs. *Clin. Neurophysiol.* **2011**, *122*, 364–372. [CrossRef] [PubMed]
38. Lew, E.; Chavarriaga, R.; Silvoni, S.; Millán, J.d.R. Detection of self-paced reaching movement intention from EEG signals. *Front. Neuroeng.* **2012**, *5*, 13. [CrossRef] [PubMed]
39. Jochumsen, M.; Petersen, B.S.; Vestergaard, L.M.; Falborg, N.F.; Wisler, L.; Olesen, M.V.; Andersen, M.S.; Sørensen, N.B.; Jørgensen, S.T. Detection of movement-related cortical potentials associated with upper and low limb movements in patients with multiple sclerosis for brain-computer interfacing. *J. Neural Eng.* **2025**, *22*, 046026. [CrossRef] [PubMed]
40. Jochumsen, M.; Sulkjær, C.S.; Dalgaard, K.S. Comparison of Classifier Calibration Schemes for Movement Intention Detection in Individuals with Cerebral Palsy for Inducing Plasticity with Brain–Computer Interfaces. *Sensors* **2025**, *25*, 7347. [CrossRef] [PubMed]
41. Dong, R.; Zhang, X.; Zhou, Z.; Zha, W.; Zhu, A. Deep spatio-temporal features optimised fusion with coordinate attention mechanism for EEG lower limb pre-movement intention decoding. *Biocybern. Biomed. Eng.* **2025**, *45*, 515–527. [CrossRef]
42. Crell, M.R.; Kostoglou, K.; Suwandjieff, P.; da Cruz, J.R.; Müller-Putz, G.R. A Non-Invasive, MRCP-Based BCI for Online Communication. *IEEE Trans. Neural Syst. Rehabil. Eng.* **2026**, *34*, 1272–1283. [CrossRef] [PubMed]
43. Zhang, J.; Shen, C.; Chen, W.; Ma, X.; Liang, Z.; Zhang, Y. Decoding of movement-related cortical potentials at different speeds. *Cogn. Neurodyn.* **2024**, *18*, 3859–3872. [CrossRef] [PubMed]
44. Pfurtscheller, G.; Neuper, C. Motor Imagery and Direct Brain–Computer Communication. *Proc. IEEE* **2001**, *89*, 1123–1134. [CrossRef]

Disclaimer/Publisher's Note: The statements, opinions and data contained in all publications are solely those of the individual author(s) and contributor(s) and not of MDPI and/or the editor(s). MDPI and/or the editor(s) disclaim responsibility for any injury to people or property resulting from any ideas, methods, instructions or products referred to in the content.